Research Square

Preprints are preliminary reports that have not undergone peer review.
They should not be considered conclusive, used to inform clinical practice,
or referenced by the media as validated information.

Dark localized waves for the (3+1)-dimensional Wazwaz-Kaur-Boussinesq equation

Tao Xu

xutaohq@163.com

Zhengzhou University of Light Industry

Haiqing Zhang

Saint Xavier University

Abdul-Majid Wazwaz

Saint Xavier University

Yaonan Shan

Zhengzhou University of Light Industry

Research Article

Keywords:

Posted Date: November 3rd, 2026

DOI: https://doi.org/10.21203/rs.3.rs-11324850/v1

License: This work is licensed under a Creative Commons Attribution 4.0 International License.
Read Full License

Additional Declarations: No competing interests reported.

Dark localized waves for the (3+1)-dimensional Wazwaz-Kaur-Boussinesq equation

Tao Xu[1*], Haiqing Zhang[1], Abdul-Majid Wazwaz[2], Yaonan Shan[1]

[1] *School of Mathematics and Information Science, Zhengzhou University of Light Industry, Zhengzhou, 450002, Henan, China*
[2] *Department of Mathematics, Saint Xavier University, Chicago, IL 60655 USA*

Abstract

Starting from the nonzero background, dark localized waves are systematacially researched in the (3+1)-dimensional Wazwaz-Kaur-Boussinesq equation by Hirota bilinear method. Firstly, the generalized bilinear form with a nonzero constant C is obtained and N-dark-soliton solutions are successfully given. Subsequently, dark resonant soliton solutions, encompassing Y-shaped and X-shaped solitons, are directly derived through choosing some appropriate resonant conditions in the received N-dark-soliton. By introducing the velocity resonance conditions to the aforementioned N-soliton, the general dark soliton molecules (SMs) are then constructed. Moreover, these SMs can be classified into three categories: pure dark SMs, dark SMs interacting with standard dark solitons, and hybrid solutions of different dark SMs. Then, the concrete expressions of M-dark-lump solutions are given by the complex conjugate and the long-wave limit methods, especially, one- and two-dark lumps are discussed in detail. Next, the interactions between different types of dark localized waves were investigated, specifically: Y-shaped solitons and solitons, lumps and solitons, and lumps interacting with breathers. Finally, the mathematical formation mechanisms and some related dynamics of these nonlinear localized waves are systematically elucidated through comprehensive analysis.

Keywords: The Wazwaz-Kaur-Boussinesq equation; Dark resonant solitons; Dark soliton molecules; Dark lump solutions; Interactional solutions.

1. Introduction

Nonlinear partial differential equations (NLPDEs) serve as a cornerstone framework in modern mathematical physics for describing complex dynamics in continuous media. And thus, the multifunctionality of NLPDEs establishes them as indispensable tools for characterizing diverse physical processes spanning plasma physics, condensed matter dynamics, fluid mechanics, and nonlinear optical systems [1–4]. A diverse array of analytical frameworks has emerged for investigating NLPDEs and prominent methodologies encompass: the Bäcklund transformation method [5, 6], Darboux transformation [7–9], inverse scattering method [10], Hirota bilinear method [11, 12], bilinear neural network method [13, 14], Riemann-Hilbert method [15], long-wave limit method [16, 17] and trial function method [18, 19], etc. Building on the advancement of analytical methods for NLPDEs, a deeper understanding of localized wave structures in nonlinear systems is expected, and novel dynamical structures are anticipated to emerge.

Nowadays, investigating dark solitons is a hot topic in the field of integrable systems [20–23]. Generally speaking, dark solitons exhibit localized intensity minima embedded within a uniform high-intensity background, characterized by wave amplitude depressions that form distinct troughs in the wave profile [22]. Dark and antidark solitons on continuous and doubly periodic backgrounds as well as their long-time asymptotic analysis were all discussed in the space-shifted nonlocal nonlinear Schrödinger equation [23]. Utilizing the KP hierarchy reduction method, both N-dark-soliton and Nth-order breathers were all generated in the coupled Sasa-Satsuma equation [24]. With the development of the Darboux transformation method, researchers have successfully derived N-elliptic-dark soliton solutions in various nonlinear systems including the nonlinear Schrödinger equation [25], the defocusing Hirota equation [26] and the defocusing Lakshmanan-Porsezian-Daniel (LPD) equation [27], to name a few. Resonant soliton, characterized by the nonlinear interactions between solitary waves and external resonant fields (e.g., optical cavities, topological waveguides, or nonlinear media), have undergone significant advancements in recent years. Based on the Hirota bilinear method, various types of resonant solitons-including Y-shaped and

*Corresponding author
Email address: xutaohq@163.com (Tao Xu[1])

X-shaped-along with their interactions with normal solitons, have been identified in different high-dimensional systems [28–30]. All resonant solitons discussed in the above literature are bright, whereas, to our knowledge, research on dark resonant solitons is scarce. Therefore, it is highly necessary to research dark solitons and dark resonant solitons in the high-dimensional systems.

Soliton molecules(SMs), recognized as an important class of nonlinear localized waves in nonlinear systems, have attracted extensive attention in recent years in fields such as optics, Bose-Einstein condensates, and hydrodynamics [31–33]. Mathematically, Lou first introduced the velocity resonant method to construct SMs in in a series of nonlinear models including the Sharma-Tasso-Olver-Burgers equation [34] and the generalized Korteweg-de Vries equation [35], etc. And then, Li generalized Lou's methods to other high-dimensional systems, such as (2+1)-dimensional B-type Kadomtsev-Petviashvili equation and (2+1)-dimensional bidirectional Sawada-Kotera equation [36, 37]. Recently, there have been many reports on dark SMs in a mass of nonlinear systems including Hirota equation [38], the mixed three-level coupled Maxwell-Bloch equations [39] and the LPD equation [40], to name a few. Building upon this foundation, broadening the research scope from SMs to dark case and elucidating their interplay with dark solitons represent critical advancements in nonlinear photonics.

Unlike solitons, lump solutions often appear in high-dimensional systems, decaying algebraically as $|x|$, $|y|$, $|z| \to \infty$ (or there may be other spatial variables) and exhibiting compact, particle-like structures in space-time [41, 42]. Generally, typical lump solutions exhibit an eye-shaped structure and can be mathematically expressed as rational functions of the independent variables [42]. In recent years, there have been many analytic methods to construct lumps in different high-dimensional systems including the positive quadratic function [42], the long-wave limit method [30], Darboux transformation [43] and KP-hierarchy reduction method [44], and so on. Compared with bright lump solutions, dark lump solutions exhibit an inverse eye-shaped structure, are more suitable for describing "missing" or "suppressed" wave phenomena, and provide new perspectives for understanding the behavior of complex nonlinear systems [45, 46]. And thus, it is of great physical significance to generalize the research on bright lump solutions to dark ones in high-dimensional nonlinear systems.

In this paper, we will mainly investigate three kinds of dark localized waves for the following (3+1)-dimensional Wazwaz-Kaur-Boussinesq (WKB) equation [47–51]

$$u_{tt} - u_{xx} - \beta(u^2)_{xx} - \gamma u_{xxxx} + \frac{\alpha^2}{4}u_{yy} + \alpha u_{yt} + \delta u_{xz} = 0, \tag{1}$$

where $u = u(x, y, z, t)$, α, β, γ and δ are arbitrary real constants, the subscripts denote the related partial derivatives. Moreover, the WKB equation (1) is also called (3+1)-dimensional Boussinesq equation, and it can explain the propagation of gravity waves over the water surface, specifically addressing the frontal collision of oblique wave profiles [47].

In [47], Wazwaz et al. first presented Eq.(1) and gave its Painlevé expansion as well as some multiple solitons. Using the bilinear neural network method [48], the authors obtained lump, single, and periodic soliton wave solutions in Eq.(1). In [49], the authors derived a range of distinct solutions, such as single, periodic, dark, and rational wave solutions. Furthermore, they also presented the bifurcation, chaotic, and sensitivity analysis for the (3+1)-dimensional WKB equation. Through F expansion method, three kinds of nonlinear localized waves were constructed in Eq.(1) [50], i.e., Jacobi elliptic solutions, bright and compound bright-complex singular solitons. In [51], the authors discussed N-soliton, lump solutions (Only the general formulas for 1 to 3 lump solutions are provided) and lump interacting with solitons for Eq.(1). By considering both the complex conjugate reduction and the long-wave limit methods [52], the semi-rational solutions including solitons-breathers and line rogue waves coexisting with solitons were systematacially studied in Eq.(1). Based on the Wronskian technique, the authors successfully generated the general Wronskian solutions which can be reduced to N-soliton and rational solutions [53]. Moreover, some traveling wave solutions, sensitivity and bifurcation analysis were all given in the above-mentioned (3+1)-dimensional WKB equation [54].

In review of Refs. [51] and [52], we identify the following two unresolved issues. First, they only provided specific forms for the first few solutions (e.g., 1 to 3 lump solutions) without presenting the general formula for arbitrary-order cases. Second, they only presented the traditional N-soliton solutions without extending to other types such as the resonant solitons and SMs. According to the above, we will generalize the study of localized waves in Eq.(1) to the dark scenario. More specifically, three kinds of dark localized waves-dark resonant solitons, general dark solitons, and dark lumps-are mainly discussed, along with their interactions. Introducing a nonzero constant C in the variable transformation, the general dark resonant solitons, including Y-shaped and X-shaped solitons, are successfully reduced from the received N-dark-soliton. Next, the general dark SMs which be classified into three categories-pure dark SMs, dark SMs interacting with standard dark solitons-are excited by choosing the appropriate velocity resonance conditions in the N-dark-soliton. Besides, the general formulas of M-dark-lump are derived through both the complex conjugate and the long-wave limit methods. Then, some interactional solutions are also demonstrated, i.e., Y-shaped solitons and solitons, lumps and solitons, and lumps interacting

with breathers. In the end, the generation mechanisms and the dynamics of these nonlinear localized waves are all given in detail.

Our paper is organized as follows. In Sect.2, multi dark solitons, Y-shaped and X-shaped resonant solitons of Eq.(1) are investigated. In Sect.3, the general dark SMs, which can be categorized into three distinct types, are generated by introducing the velocity resonance conditions in the received N-dark-soliton. In Sect.4, the concrete expressions of arbitrary M-dark-lump solutions are constructed by the complex conjugate and the long-wave limit methods. In Sect.5, the interactions between different types of dark localized waves were investigated, i.e., Y-shaped solitons and standard solitons, lumps and solitons, and lumps interacting with breathers. In the last section, it is concluded with some summaries and discussions

2. N-dark-soliton and M-dark-resonant-soliton for the (3+1)-dimensional WKB equation

Generally, bright solitons are typically excited from a zero background plane, whereas dark solitons arise from a non-zero background. Introducing a nonzero constant C in the variable transformation, we derive N-dark-soliton for Eq.(1) in form of the celebrated exponential function through the Hirota bilinear method. And then, M-dark-resonant-soliton solutions (Y- and X-shaped resonant solitons) are subtly reduced from the above-mentioned N-dark-soliton by choosing some appropriate resonant conditions. Furthermore, the anti-dark types of the three localized waves obtained above, including anti-dark N-soliton and anti-dark resonant solitons, are additionally provided.

To smoothly obtain dark solitons, we select the following dependent variable transformation

$$u = v + C, \tag{2}$$

where v=$v(x, y, z, t)$, C is an arbitrary non-zero real constant, and then, Eq.(1) can be cast into the new equation

$$v_{tt} - (1 + 2C\beta)v_{xx} - \beta(v^2)_{xx} - \gamma v_{xxxx} + \frac{\alpha^2}{4}v_{yy} + \alpha v_{yt} + \delta v_{xz} = 0. \tag{3}$$

Introducing $v = q_x$ in Eq.(3) and integrating both sides of it, we can naturally have

$$q_{tt} - (1 + 2C\beta)q_{xx} - 2\beta q_x q_{xx} - \gamma q_{xxxx} + \frac{\alpha^2}{4}q_{yy} + \alpha q_{yt} + \delta q_{xz} = 0, \tag{4}$$

with q=$q(x, y, z, t)$. Introducing the Cole-Hopf transformation q=$k(lnf)_x$ in Eq.(4), where k is a real constant and f=$f(x, y, z, t)$, we can get k=$\frac{6\gamma}{\beta}$ by comparing the coefficients of the higher-order nonlinear terms. Therefore, $v = \frac{6\gamma}{\beta}(lnf)_{xx}$.

In summary, under the received dependent variable transformation

$$u = \frac{6\gamma}{\beta}(\ln f)_{xx} + C, \tag{5}$$

and thus Eq.(1) can be directly transformed into the following bilinear form

$$(\gamma D_x^4 + (1 + 2C\beta)D_x^2 - D_t^2 - \frac{\alpha^2}{4}D_y^2 - \alpha D_y D_t - \delta D_x D_z)f \cdot f = 0, \tag{6}$$

where D denotes the Hirota's bilinear operator and is given as

$$\begin{aligned} &D_x^k D_y^l D_z^m D_t^n h(x, y, z, t) \cdot g(x, y, z, t) \\ &= \Big(\frac{\partial}{\partial_x} - \frac{\partial}{\partial_{x'}}\Big)^k \Big(\frac{\partial}{\partial_y} - \frac{\partial}{\partial_{y'}}\Big)^l \Big(\frac{\partial}{\partial_z} - \frac{\partial}{\partial_{z'}}\Big)^m \Big(\frac{\partial}{\partial_t} - \frac{\partial}{\partial_{t'}}\Big)^n h(x, y, z, t) \times g(x', y', z', t')|_{x=x', y=y', z=z', t=t'}, \end{aligned}$$

and $k,\ l,\ m,\ n$ are all positive integers.

In review of the procedures in [55], the N-dark-soliton solutions of Eq.(1) are successfully derived in the following celebrated exponential form

$$u = \frac{6\gamma}{\beta}\Big(\ln\Big(\sum_{\mu=0,1}\exp\Big(\sum_{i=1}^{N}\mu_i\eta_i + \sum_{1\le i<j}^{N}\mu_i\mu_j A_{ij}\Big)\Big)\Big)_{xx} + C\ (1\le i<j\le N), \tag{7}$$

with

$$\eta_i = \omega_i t + k_i x + p_i y + q_i z + \eta_i^0, \tag{8}$$

$$\omega_i = -\frac{p_i \alpha}{2} + \sqrt{k_i^4 \gamma - k_i q_i \delta + (1 + 2C\beta)k_i^2}, \tag{9}$$

$$e^{A_{ij}} = \frac{\xi - \delta(k_i q_j + k_j q_i) - 6\gamma k_i^2 k_j^2}{\xi - \delta(k_i q_j + k_j q_i) + 6\gamma k_i^2 k_j^2}, \tag{10}$$

$$\xi = -2\sqrt{k_i k_j(\gamma k_j^3 - \delta q_j + (1 + 2C\beta)k_j)(\gamma k_i^3 - \delta q_i + (1 + 2C\beta)k_i)} + 2k_i k_j(2\gamma k_i^2 + 2\gamma k_j^2 + 1 + 2C\beta). \tag{11}$$

where k_i, p_i, q_i and η_i^0 are all arbitrary real constants. Observing Eq.(5), one can easily find that soliton type is controlled by these three constants β, γ and C. For convenience of discussion, we choose that γ>0 and C>0, and depending on the sign of β, dark solitons (β<0) and anti-dark solitons (β>0) can be obtained.

Setting N=1 in Eq.(7) and choosing the same values of these free constants (see the caption in Fig.1) except for β, we can get one-dark-soliton solotion with β=−1 as

$$u_{one-dark} = \frac{40\cosh(y + \frac{3}{4}z - 1) - 32}{60\cosh^2(y + \frac{3}{4}z - 1)}. \tag{12}$$

Similar to the above case, the expression of one-anti-dark-soliton with β=1 can be also derived as

$$u_{one-anti-dark} = \frac{40\cosh(y + \frac{3}{4}z - 1) + 112}{60\cosh^2(y + \frac{3}{4}z - 1)}. \tag{13}$$

As shown in Fig.1(a), this soliton exhibits a downward notch from a positive non-zero background, and its minimum amplitude remains greater than 0, which is assuredly a dark soliton. Unlike traditional bright solitons excited from a zero background, the soliton in Fig.1(b) exhibits an upward hump (or peak) from a positive non-zero background, a structure widely referred to as an anti-dark soliton. To verify the universality of our formulas, we derive two- to four-soliton solutions, respectively, and only give some figures to demonstrate the related dynamics, see Figs.2-4.

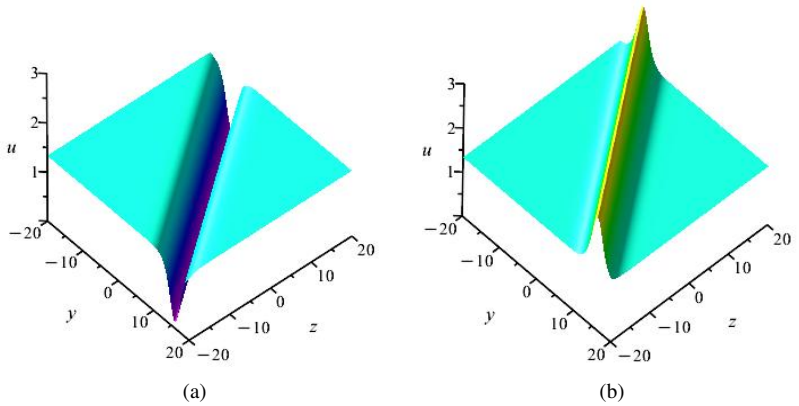


Fig. 1: One-soliton solution with the parameters chosen by $k_1 = -1$, $p_1 = 1$, $q_1 = \frac{3}{4}$, $\alpha = \frac{1}{2}$, $\gamma = \frac{4}{5}$, $\delta = \frac{3}{2}$, $\eta_1^0 = 0$, $x = 1$, $t = 0$, $C = \frac{4}{3}$: (a) one-dark-soliton ($\beta = -1$); (b) one-anti-dark-soliton ($\beta = 1$).

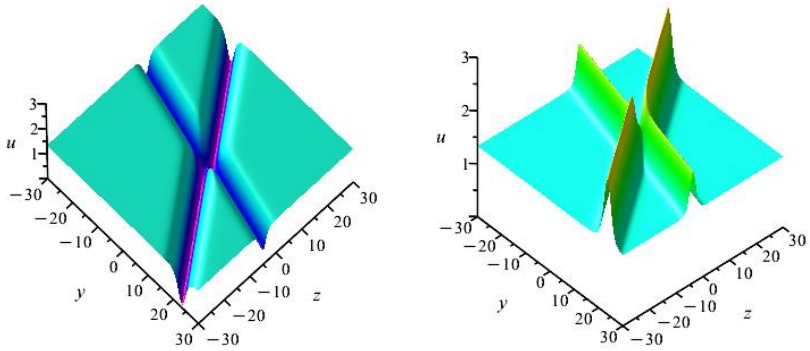


Fig. 2: Two-soliton solutions with the parameters chosen by $k_1 = -1$, $k_2 = -\frac{4}{5}$, $p_1 = 1$, $p_2 = \frac{1}{3}$, $q_1 = \frac{3}{4}$, $q_2 = \frac{4}{3}$, $\alpha = \frac{1}{2}$, $\gamma = \frac{4}{5}$, $\delta = \frac{3}{2}$, $\eta_1^0 = 0$, $\eta_2^0 = 0$, $x = 1$, $t = 0$, $C = \frac{4}{3}$: (a) two-dark-soliton ($\beta = -1$); (b) two-anti-dark-soliton($\beta = 1$).

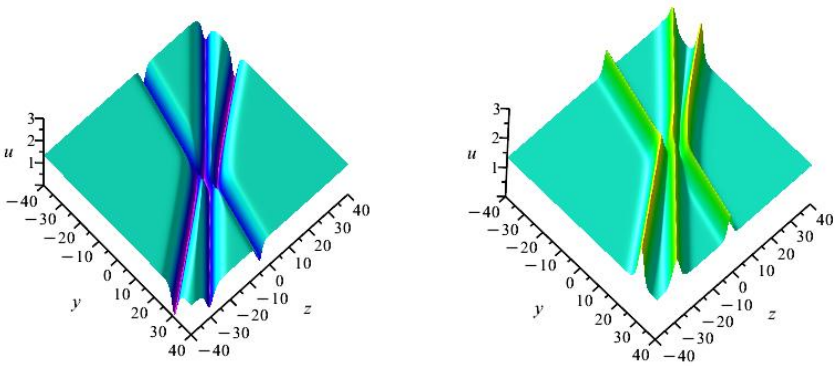


Fig. 3: Three-soliton solutions with the parameters chosen by $k_1 = -1$, $k_2 = -\frac{4}{5}$, $k_3 = -\frac{5}{6}$, $p_1 = 1$, $p_2 = \frac{1}{3}$, $p_3 = \frac{3}{4}$, $q_1 = \frac{3}{4}$, $q_2 = \frac{4}{3}$, $q_3 = \frac{4}{5}$, $\alpha = \frac{1}{2}$, $\gamma = \frac{4}{5}$, $\delta = \frac{3}{2}$, $\eta_1^0 = 0$, $\eta_2^0 = 0$, $\eta_3^0 = 0$, $x = 1$, $t = 0$, $C = \frac{4}{3}$: (a) three-dark-soliton ($\beta = -1$); (b) three-anti-dark-soliton ($\beta = 1$).

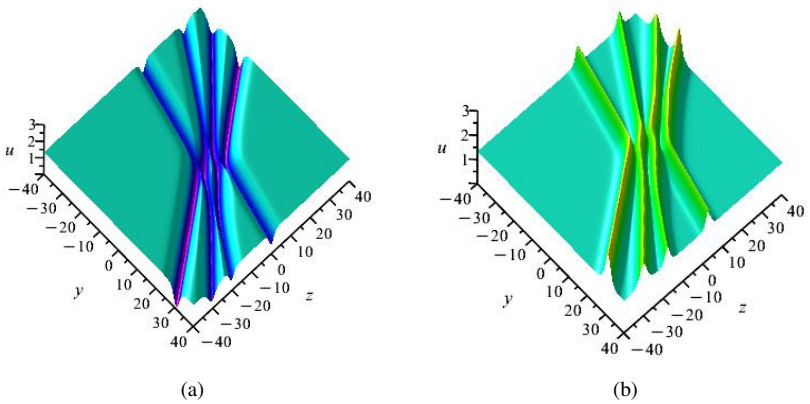


Fig. 4: Four-soliton solutions with the parameters chosen by $k_1 = -1$, $k_2 = -\frac{4}{5}$, $k_3 = -\frac{5}{6}$, $k_4 = -\frac{3}{4}$, $p_1 = 1$, $p_2 = \frac{1}{3}$, $p_3 = \frac{3}{4}$, $p_4 = \frac{4}{5}$, $q_1 = \frac{3}{4}$, $q_2 = \frac{4}{3}$, $q_3 = \frac{4}{5}$, $q_4 = \frac{5}{4}$, $\alpha = \frac{1}{2}$, $\gamma = \frac{4}{5}$, $\delta = \frac{3}{2}$, $\eta_1^0 = 0$, $\eta_2^0 = 0$, $\eta_3^0 = 0$, $\eta_4^0 = 0$, $x = 1$, $t = 0$, $C = \frac{4}{3}$: (a) four-dark-soliton ($\beta = -1$); (b) four-anti-dark-soliton ($\beta = 1$).

Fundamentally, resonant solitons enable energy-efficient broadband microcombs in resonantly-coupled microresonators and stabilize matter-wave configurations in Bose-Einstein condensates, thereby advancing optical signal processing architectures and unlocking potential for high-speed data transmission and quantum computing applications [56, 57]. Recently, the resonant solitons have been actively investigated in different high-dimensional integrable systems [28–30]. To our knowledge, most existing reports on resonant solitons focus on bright cases, while research on dark resonant solitons remains scarce. In the following, we will reduce the concrete expressions of M-dark-resonant-soliton solutions, including Y-shaped and X-shaped solitons, from the above-mentioned N-dark-soliton solutions.

(1) M-dark-resonant-Y-shaped-soliton solutions

When the phase shift of colliding solitons equals or tends to infinity, naturally generated resonant solitons attain their maximum amplitudes and undergo significant energy conversion [56, 57]. In review of Eq.(7), the criterion for the phase shift between solitons to tend to infinity can be determined by $e^{A_{ij}}$=0. Starting from two-soliton solution (choosing N=2 in Eq.(7)), the resonance phenomenon of two solitons-namely the Y-shaped soliton structure-can occur with the resonance condition $e^{A_{12}}$=0, i.e.,

$$q_2 = \frac{2\gamma k_2(k_1^2 - 3k_1k_2 + 2k_2^2)}{\delta} + \frac{k_2 q_1}{k_1} - \frac{2k_2\sqrt{-3\gamma k_1^3(k_1-k_2)^2(\gamma k_1^3 + 2C\beta k_1 - \delta q_1 + k_1)}}{k_1^2\delta}, \tag{14}$$

here, q_2 is an arbitrary real constant, naturally requiring that $\gamma k_1^3(\gamma k_1^3 + 2C\beta k_1 - \delta q_1 + k_1) < 0$.

Considering the aforementioned conditions, we set γ<0 without loss of generality, and thus, one-dark- (β>0) and one-anti-dark-resonant-Y-shaped-soliton (β<0) can be successfully generated, respectively. Choosing N=2 in the Eq.(7) and fixing freedom parameters (refer to the caption of Fig.5(a)), the explicit expression of one-dark-resonant-Y-shaped-soliton admits

$$u_{one-dark-Y} = \frac{14e^{a_1+a_2} + 9e^{2a_1} + 9e^{2a_2} - 18e^{a_1} + 2e^{a_2} + 9}{3(1 + e^{a_1} + e^{a_2})^2}, \tag{15}$$

where

$$a_1 = \frac{3y}{2} + \frac{z}{3} + 1, a_2 = \frac{2y}{3} - \frac{2\sqrt{114}z}{9} + \frac{2}{3}.$$

As shown in Fig.5(a), the two dark solitons on the left (upper and lower) form a single deeper valley and constitute a Y-shaped dark soliton after resonant interaction. Similar to one-dark-Y-shaped-resonant-soliton, the dark case can also be obtained with the parameters chosen in the caption of Fig.5(b), and it holds

$$u_{one-anti-dark-Y} = \frac{7e^{a_3+a_4} + 2e^{2a_3} + 2e^{2a_4} + 16e^{a_3} + 7e^{a_4} + 9}{(1 + e^{a_3} + e^{a_4})^2}, \tag{16}$$

with

$$a_3 = y + \frac{3z}{2} + 1, a_4 = y + \frac{3z}{4} + \frac{1}{2}.$$

In contrast to Fig.5(a), Fig.5(b) displays a protruding Y on a non-zero background plane, which we refer to as the anti-dark Y-shaped soliton.

Similar to multi solitons, we can construct interactions between multi Y-shaped solitons. Starting from $2M$ solitons (choosing N=$2M$ in Eq.(7)), the concrete expressions of M-dark-resonant-Y-shaped-soliton (or anti-dark cases) can be obtained with following resonance conditions in Eq.(7)

$$e^{A_{2m-1,2m}} = 0 \ (1 \le m \le M), \tag{17}$$

where the terms of $e^{A_{2m-1,2m}}$ have been all given in Eq.(10).

(2) M-dark-resonant-X-shaped-soliton solutions

As discussed above, we have examined pairwise resonance among an even number of solitons. Subsequently, we shift our focus to the resonant behavior of an odd number of solitons. Taking three solitons as an example (choosing N=3 in Eq.(7)), one can get the X-shaped resonant soliton by introducing the following resonant condi-

tions $e^{A_{12}}$=$e^{A_{13}}$ = 0 in three-soliton, i.e.,

$$q_2 = \frac{2\gamma k_2(k_1^2 - 3k_1k_2 + 2k_2^2)}{\delta} + \frac{k_2 q_1}{k_1} - \frac{2k_2\sqrt{-3\gamma k_1^3(k_1-k_2)^2(\gamma k_1^3 + 2C\beta k_1 - \delta q_1 + k_1)}}{k_1^2\delta}, \tag{18}$$

$$q_3 = \frac{2\gamma k_3(k_1^2 - 3k_1k_3 + 2k_3^2)}{\delta} + \frac{k_3 q_1}{k_1} - \frac{2k_3\sqrt{-3\gamma k_1^3(k_1-k_3)^2(\gamma k_1^3 + 2C\beta k_1 - \delta q_1 + k_1)}}{k_1^2\delta}. \tag{19}$$

where $\gamma k_1^3(\gamma k_1^3 + 2C\beta k_1 - \delta q_1 + k_1) < 0$.

Analogous to the resonant Y-shaped soliton, a dark X-shaped soliton can be derived by setting γ<0, β>0; the corresponding anti-dark counterpart is then obtained when γ<0, β<0. As shown in Fig.6(a), dark soliton 2 (S_2) and dark soliton 1 (S_1) undergo resonance to form a more deeply indented resonant soliton 1 (RS_1), collectively forming a configuration that resembles the letter "Y". Besides, Similarly, dark soliton 1 (S_1) engages in resonance with dark soliton 3 (S_3), giving rise to a second resonant soliton (RS_2) and forming another distinct Y-shaped structure. Solitons 2 (S_2) and 3 (S_3) both interact through soliton 1 (S_1). Upon their mutual resonance, they form an irregular X-shaped structure, which we term the X-shaped resonant soliton. The anti-dark X-type resonant soliton can also be obtained through a similar process, which we will not discuss in detail, see Fig.6(b).

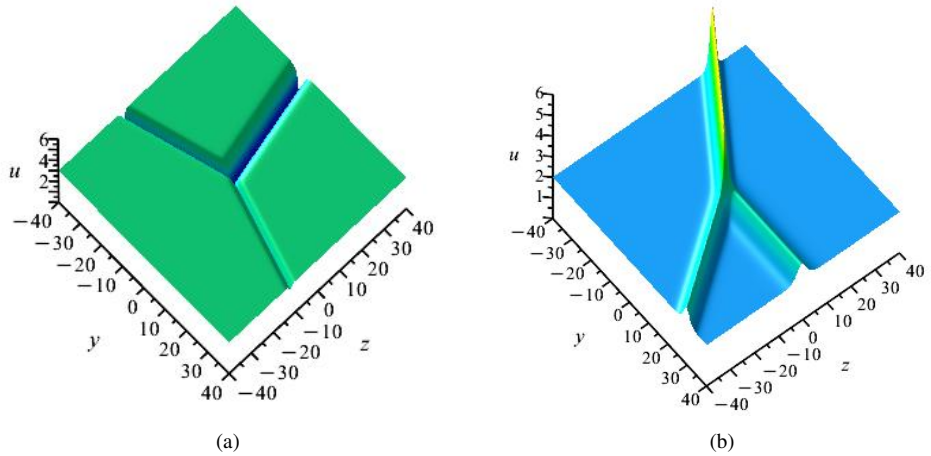
Starting from $2M$+1 solitons (odd number of solitons), the concrete expressions of M-resonant-X-shaped-soliton-including dark and anti-dark cases-can also be derived by introducing the following resonance conditions in Eq.(7), namely,

$$e^{A_{1,s}} = 0\ (2 \le s \le 2M{+}1), \tag{20}$$

and specifically,

$$q_s = \frac{2\gamma k_s(k_1^2 - 3k_1k_s + 2k_s^2)}{\delta} + \frac{k_s q_1}{k_1} - \frac{2k_s\sqrt{-3\gamma k_1^3(k_1-k_s)^2(\gamma k_1^3 + 2C\beta k_1 - \delta q_1 + k_1)}}{k_1^2\delta}, \tag{21}$$

with $\gamma k_1^3(\gamma k_1^3 + 2C\beta k_1 - \delta q_1 + k_1) < 0$.



(a) (b)

Fig. 5: (a)The dark Y-shaped resonant soliton solutions with the parameters chosen by $k_1 = 1, k_2 = \frac{2}{3}, p_1 = \frac{3}{2}, p_2 = \frac{2}{3}, q_1 = \frac{1}{3}, q_2 = -\frac{2\sqrt{114}}{9}, \alpha = 1, \beta = \frac{1}{4}, \gamma = -\frac{1}{2}, \delta = -\frac{1}{3}, \eta_1^0 = 0, \eta_2^0 = 0, x = 1, t = 0, C = 3$; (b)The anti-dark Y-shaped resonant soliton solutions with the parameters chosen by $k_1 = 1, k_2 = \frac{1}{2}, p_1 = 1, p_2 = 1, q_1 = \frac{3}{2}, q_2 = \frac{3}{4}, \alpha = 1, \beta = -\frac{1}{4}, \gamma = -\frac{1}{2}, \delta = -\frac{1}{3}, \eta_1^0 = 0, \eta_2^0 = 0, x = 1, t = 0, C = 2$.

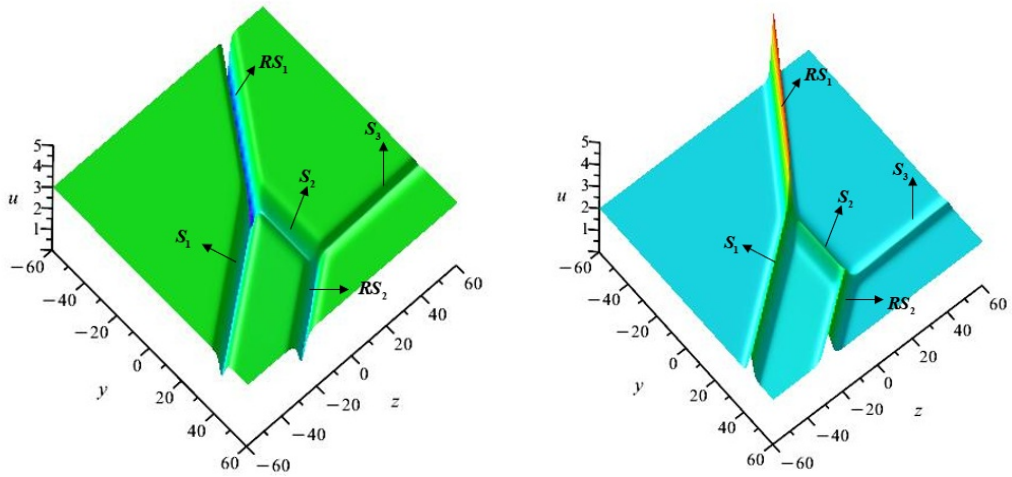


Fig. 6: The X-shaped resonant soliton solutions with the parameters chosen by $k_1 = 1$, $k_2 = \frac{1}{2}$, $k_3 = \frac{2}{3}$, $p_1 = 1$, $p_2 = 1$, $p_3 = 1$, $q_1 = \frac{3}{2}$, $\alpha = 1$, $\gamma = -\frac{1}{2}$, $\delta = -\frac{1}{3}$, $\eta_1^0 = 0$, $\eta_2^0 = 0$, $\eta_3^0 = 0$, $x = 1$ $t = 0$: (a)dark X-shaped resonant soliton solution : $q_2 = \frac{3-3\sqrt{15}}{4}$, $q_3 = \frac{7-6\sqrt{15}}{9}$, $\beta = \frac{1}{4}$, $C = 3$; (b)anti-dark X-shaped resonant soliton solution : $q_2 = \frac{3}{4}$, $q_3 = \frac{7}{9}$, $\beta = -\frac{1}{4}$, $C = 2$.

3. The general dark soliton molecules for the (3+1)-dimensional WKB equation

Compared with traditional soliton solutions, SMs exhibit more complex structures and dynamics, offering the potential to encode richer information in optical communications. In recent years, research efforts have predominantly focused on bright SMs [31–37], with relatively few studies dedicated to dark SMs. Given the facts above, it is greatly necessary and meaningful to generate the bright SMs to dark case in nonlinear photonics. Subsequently, we will investigate the general SMs of Eq.(1), which can be classified into three categories: pure dark SMs, dark SMs interacting with standard dark solitons, and hybrid solutions of different dark SMs.

In review of Eq.(7), one can easily derive the velocities of the i-th soliton ($1 \leq i \leq N$) along the x- and y-axes, respectively,

$$V_{i,x} = -\frac{\omega_i}{k_i} = \frac{\frac{p_i\alpha}{2} - \sqrt{k_i^4\gamma - k_i q_i \delta + (1+2C\beta)k_i^2}}{k_i}, \tag{22}$$

$$V_{i,y} = -\frac{\omega_i}{p_i} = \frac{\frac{p_i\alpha}{2} - \sqrt{k_i^4\gamma - k_i q_i \delta + (1+2C\beta)k_i^2}}{p_i}. \tag{23}$$

It is well established that SMs emerge when the propagation velocities of individual solitons along specific directions are identical. Taking the two-dark-soliton case as an example, one dark SM phenomenon appears when $V_{1,x}=V_{2,x}$ and $V_{1,y}=V_{2,y}$, where z is chosen as a constant. For simplicity, we named this kind of dark SM generated by two solitons as 2-dark-SMs. Similarly, M-dark-SMs ($2 \leq M \leq N$) constitute an interaction complex formed by M dark solitons sharing identical velocities along the x- and y-axes.

Choosing any M solitons in N-soliton in Eq.(7), we label their velocities along the x- and y-axes as ($V_{1,x}^{(l)}$, $V_{2,x}^{(l)}$, $\cdots$, $V_{M-1,x}^{(l)}$, $V_{M,x}^{(l)}$) and ($V_{1,y}^{(l)}$, $V_{2,y}^{(l)}$, $\cdots$, $V_{M-1,y}^{(l)}$, $V_{M,y}^{(l)}$), where $2 \leq M \leq N$. More specially, these symbols "$_1^{(l)}$, $_2^{(l)}$, $\cdots$, $_{M-1}^{(l)}$, $_M^{(l)}$" are any sub-permutation of this array of $(1, 2, \cdots, N)$. Without loss of generality, we assume that "$_1^{(l)} <_2^{(l)} < \cdots <_{M-1}^{(l)} <_M^{(l)}$". As alluded to above, the general dark M-SMs-($N-M$)-soliton solutions, which include M-dark-SMs and ($N-M$)-dark-soliton, can be derived from Eq.(7) with the following restricted conditions

$$V_{1,x}^{(l)} = V_{2,x}^{(l)} = \cdots = V_{M-1,x}^{(l)} = V_{M,x}^{(l)}, \tag{24}$$

$$V_{1,y}^{(l)} = V_{2,y}^{(l)} = \cdots = V_{M-1,y}^{(l)} = V_{M,y}^{(l)}, \tag{25}$$

with

$$V_{i,x}^{(l)} = -\frac{\omega_i^{(l)}}{k_i^{(l)}} = \frac{\frac{p_i^{(l)}\alpha}{2} - \sqrt{k_i^{(l)4}\gamma - k_i^{(l)}q_i^{(l)}\delta + (1+2C\beta)k_i^{(l)2}}}{k_i^{(l)}},$$
$$V_{i,y}^{(l)} = -\frac{\omega_i^{(l)}}{p_i^{(l)}} = \frac{\frac{p_i^{(l)}\alpha}{2} - \sqrt{k_i^{(l)4}\gamma - k_i^{(l)}q_i^{(l)}\delta + (1+2C\beta)k_i^{(l)2}}}{p_i^{(l)}} \ (1 \le i \le M).$$

Considering Eqs.(7), (24) and (25), the general dark M-SMs-($N-M$)-soliton solutions admit

$$\begin{cases} u_{SMs} = \frac{6\gamma}{\beta}\Big(ln\Big(\sum\limits_{\mu=0,1}\exp\big(\sum\limits_{i=1}^{N}\mu_i\eta_i + \sum\limits_{1\le i<j}^{N}\mu_i\mu_j A_{ij}\big)\Big)\Big)_{xx} + C, \\ \eta_i = (-\frac{p_i\alpha}{2} + \sqrt{k_i^4\gamma - k_iq_i\delta + (1+2C\beta)k_i^2})t + k_ix + p_iy + q_iz + \eta_i^0, \\ e^{A_{ij}} = \frac{-2\sqrt{k_ik_j(\gamma k_j^3 - \delta q_j + (1+2C\beta)k_j)(\gamma k_i^3 - \delta q_i + (1+2C\beta)k_i)} + 2k_ik_j(2\gamma k_i^2 + 2\gamma k_j^2 + 1 + 2C\beta) - \delta(k_iq_j + k_jq_i) - 6\gamma k_i^2k_j^2}{-2\sqrt{k_ik_j(\gamma k_j^3 - \delta q_j + (1+2C\beta)k_j)(\gamma k_i^3 - \delta q_i + (1+2C\beta)k_i)} + 2k_ik_j(2\gamma k_i^2 + 2\gamma k_j^2 + 1 + 2C\beta) - \delta(k_iq_j + k_jq_i) + 6\gamma k_i^2k_j^2}, \\ \frac{p_1\alpha}{2} - \sqrt{k_1^4\gamma - k_1q_1\delta + (1+2C\beta)k_1^2}}{k_1} = \frac{\frac{p_2\alpha}{2} - \sqrt{k_2^4\gamma - k_2q_2\delta + (1+2C\beta)k_2^2}}{k_2} = \cdots = \frac{\frac{p_M\alpha}{2} - \sqrt{k_M^4\gamma - k_Mq_M\delta + (1+2C\beta)k_M^2}}{k_M}, \\ \frac{p_1\alpha}{2} - \sqrt{k_1^4\gamma - k_1q_1\delta + (1+2C\beta)k_1^2}}{p_1} = \frac{\frac{p_2\alpha}{2} - \sqrt{k_2^4\gamma - k_2q_2\delta + (1+2C\beta)k_2^2}}{p_2} = \cdots = \frac{\frac{p_M\alpha}{2} - \sqrt{k_M^4\gamma - k_Mq_M\delta + (1+2C\beta)k_M^2}}{p_M}. \end{cases} \tag{26}$$

(1) N-dark-SMs

Choosing M=N in Eq.(26), one can get the pure N-dark SMs. When N=2, we can obtain 2-dark-SMs ($V_{1,x}$=$V_{2,x}$, $V_{1,y}$=$V_{2,y}$) with the non-singular condition $\gamma k_1^3(\gamma k_1^3 + 2C\beta k_1 - \delta q_1 + k_1)$<0 and $\gamma k_2^3(\gamma k_2^3 + 2C\beta k_2 - \delta q_2 + k_2)$<0. Here, the 2-dark-SMs can be derived in Fig.7(a) by setting γ<0, β>0; the corresponding anti-dark case is shown in Fig.7(b) when γ<0, β<0. As shown in Fig.7, the 2-SMs propagate in a stripe-like, wave-like manner, without undergoing significant phase shifts as observed in the traditional two-soliton in Fig.2. Specifically, Fig.7(a) shows two dark stripe structures, while Fig.7(b) corresponds to the anti-dark case. Similarly to the case of 2-SMs, we can also obtain 3- and 4-SMs characterized by three and four stripes, respectively, in both dark and anti-dark forms (refer to Figs.8 and 9).

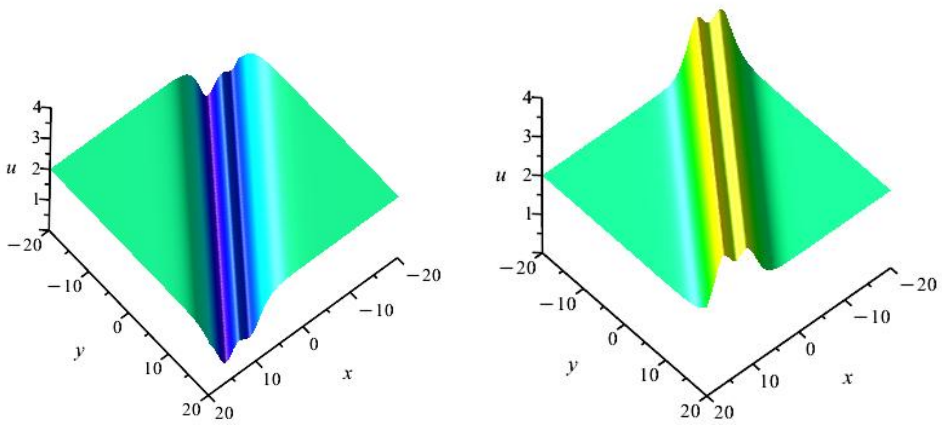


Fig. 7: (a) 2-dark-SMs solutions with the parameters chosen by $k_1 = -\frac{2}{3}$, $k_2 = -1$, $p_1 = \frac{1}{2}$, $p_2 = \frac{3}{4}$, $q_1 = \frac{3}{4}$, $q_2 = \frac{211}{216}$, $\alpha = \frac{1}{2}$, $\beta = -\frac{1}{3}$, $\gamma = \frac{2}{5}$, $\delta = \frac{3}{2}$, $\eta_1^0 = 0$, $\eta_2^0 = 0$, $z = 1$, $t = 0$, $C = 2$; (b) 2-anti-dark-SMs solutions with the parameters chosen by $k_1 = -\frac{2}{3}$, $k_2 = -1$, $p_1 = \frac{1}{2}$, $p_2 = \frac{3}{4}$, $q_1 = \frac{3}{4}$, $q_2 = \frac{179}{216}$, $\alpha = \frac{1}{2}$, $\beta = \frac{2}{3}$, $\gamma = \frac{4}{5}$, $\delta = \frac{3}{2}$, $\eta_1^0 = 0$, $\eta_2^0 = 0$, $z = 1$, $t = 0$, $C = 2$.

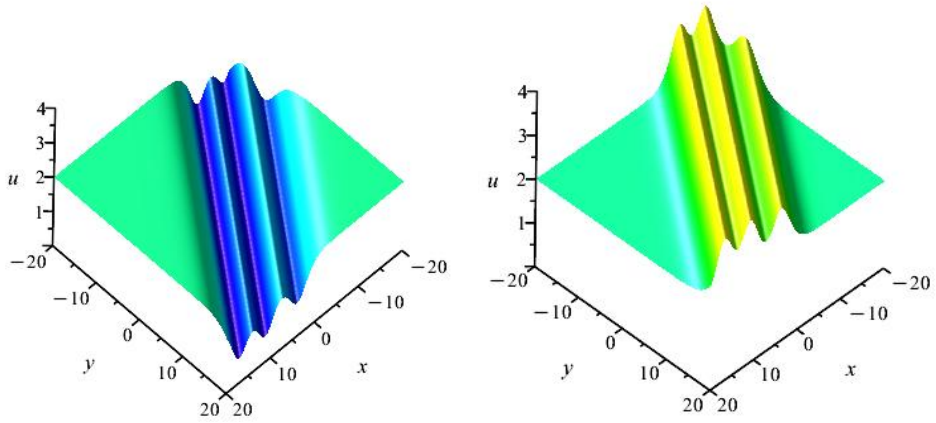


Fig. 8: (a) 3-dark-SMs solutions with the parameters chosen by $k_1 = -\frac{2}{3}, k_2 = -1, k_3 = -\frac{5}{6}, p_1 = \frac{1}{2}, p_2 = \frac{3}{4}, p_3 = \frac{5}{8}, q_1 = \frac{3}{4}, q_2 = \frac{211}{216}, q_3 = \frac{127}{144}, \alpha = \frac{1}{2}, \beta = -\frac{1}{3}, \gamma = \frac{2}{5}, \delta = \frac{3}{2}, \eta_1^0 = 0, \eta_2^0 = 0, \eta_3^0 = 0, z = 1, t = 0, C = 2$; (b) 3-anti-dark-SMs solutions with the parameters chosen by $k_1 = -\frac{2}{3}, k_2 = -1, k_3 = -\frac{5}{6}, p_1 = \frac{1}{2}, p_2 = \frac{3}{4}, p_3 = \frac{5}{8}, q_1 = \frac{3}{4}, q_2 = \frac{179}{216}, q_3 = \frac{119}{144}, \alpha = \frac{1}{2}, \beta = \frac{2}{3}, \gamma = \frac{4}{5}, \delta = \frac{3}{2}, \eta_1^0 = 0, \eta_2^0 = 0, \eta_3^0 = 0, z = 1, t = 0, C = 2$.

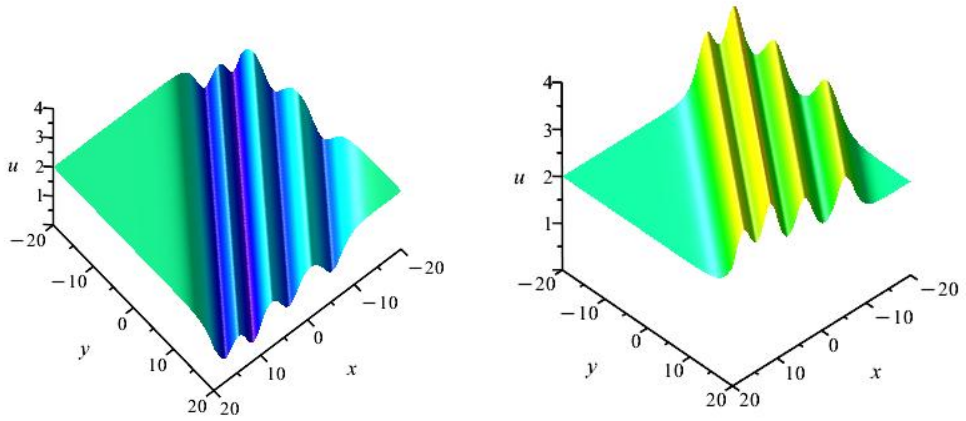


Fig. 9: (a) 4-dark-SMs solutions with the parameters chosen by $k_1 = -\frac{2}{3}, k_2 = -1, k_3 = -\frac{5}{6}, k_4 = -\frac{3}{4}, p_1 = \frac{1}{2}, p_2 = \frac{3}{4}, p_3 = \frac{5}{8}, p_4 = \frac{9}{16}, q_1 = \frac{3}{4}, q_2 = \frac{211}{216}, q_3 = \frac{127}{144}, q_4 = \frac{1181}{1140}, \alpha = \frac{1}{2}, \beta = -\frac{1}{3}, \gamma = \frac{2}{5}, \delta = \frac{3}{2}, \eta_1^0 = 0, \eta_2^0 = 0, \eta_3^0 = 0, \eta_4^0 = 0, z = 1, t = 0, C = 2$; (b) 4-anti-dark-SMs solutions with the parameters chosen by $k_1 = -\frac{2}{3}, k_2 = -1, k_3 = -\frac{5}{6}, k_4 = -\frac{3}{4}, p_1 = \frac{1}{2}, p_2 = \frac{3}{4}, p_3 = \frac{5}{8}, p_4 = \frac{9}{16}, q_1 = \frac{3}{4}, q_2 = \frac{179}{216}, q_3 = \frac{119}{144}, q_4 = \frac{1147}{1140}, \alpha = \frac{1}{2}, \beta = \frac{2}{3}, \gamma = \frac{4}{5}, \delta = \frac{3}{2}, \eta_1^0 = 0, \eta_2^0 = 0, \eta_3^0 = 0, \eta_4^0 = 0, z = 1, t = 0, C = 2$.

(2) Interactions between M-dark-SMs and $(N-M)$-dark-soliton

Fixing $2 \leq M < N$ in Eq.(26), the general dark M-SMs-$(N-M)$-soliton solutions consisting of one M-dark-SMs and $(N-M)$ traditional dark solitons can be generated. For three-soliton, we can choose two or all three solitons to own identical velocities. Once three solitons have the same velocity, the 3-SMs phenomenon appears, see Fig.8. When two solitons share the same velocity while the remaining one has a different velocity, we can get mixed solutions including a 2-SMs and a single soliton, and we refer to this solution as 2-SMs-1-soliton. As shown in Fig.10(a), the vertically oriented pair of double stripes in the depression corresponds precisely to the dark 2-SMs, while the horizontally aligned structure represents a standard single dark soliton; a similar anti-dark scenario is illustrated in Fig.10(b).

For the four-soliton case, the configurations can be categorized into the following three distinct cases: all four solitons sharing an identical velocity, three solitons sharing an identical velocity, and two solitons sharing a common velocity. When four solitons have the common velocity, the 4-SMs appear and have been given in

Fig.9. In the following, we mainly discuss the remaining two cases that three or two solitons' velocities are the same, for convenience, we call them 3-SMs-1-soliton and 2-SMs-2-soliton, respectively, see Figs.11 and 12. In Fig.11(a), the notched vertical triple stripes represent the 3-dark-SMs, and the horizontal stripe is a single dark soliton. They undergo an elastic collision characteristic of multi-soliton dynamics. Besides, the similar anti-dark case is demonstrated in Fig.11(b). It is shown that the 2-SMs-2-soliton solutions consisting of one 2-SMs and two traditional solitons in Fig.12. Evidently, the parallel, notched double stripes at the center of Fig.12(a) correspond to a dark 2-SMs, while the X-shaped structures spanning across both sides represent two dark solitons. A similar scenario is observed for the anti-dark case in Fig.12(b).

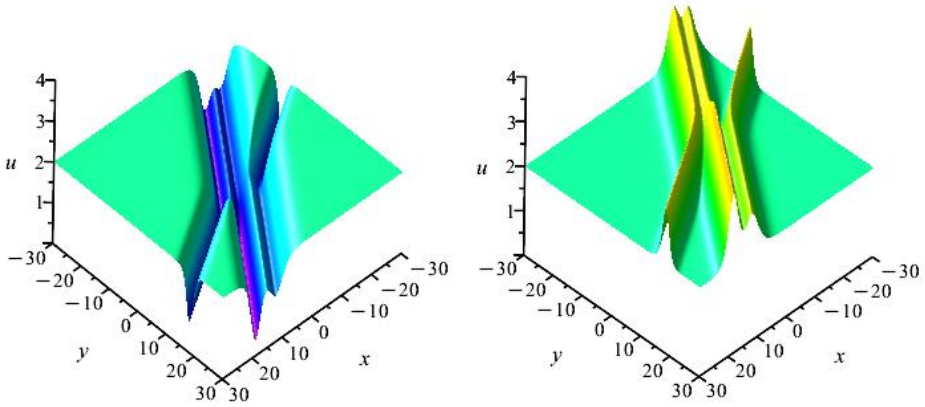


Fig. 10: (a) The dark 2-SMs-1-soliton solutions with the parameters chosen by $k_1 = -\frac{2}{3}, k_2 = -1, k_3 = -\frac{5}{6}, p_1 = \frac{1}{2}, p_2 = \frac{3}{4}, p_3 = \frac{4}{3}, q_1 = \frac{3}{4}, q_2 = \frac{211}{216}, q_3 = \frac{4}{5}, \alpha = \frac{1}{2}, \beta = -\frac{1}{3}, \gamma = \frac{2}{5}, \delta = \frac{3}{2}, \eta_1^0 = 0, \eta_2^0 = 0, \eta_3^0 = 0, z = 1, t = 0, C = 2$; (b) The anti-dark 2-SMs-1-soliton solutions with the parameters chosen by $k_1 = -\frac{2}{3}, k_2 = -1, k_3 = -\frac{5}{6}, p_1 = \frac{1}{2}, p_2 = \frac{3}{4}, p_3 = \frac{4}{3}, q_1 = \frac{3}{4}, q_2 = \frac{179}{216}, q_3 = 1, \alpha = \frac{1}{2}, \beta = \frac{2}{3}, \gamma = \frac{4}{5}, \delta = \frac{3}{2}, \eta_1^0 = 0, \eta_2^0 = 0, \eta_3^0 = 0, z = 1, t = 0, C = 2$.

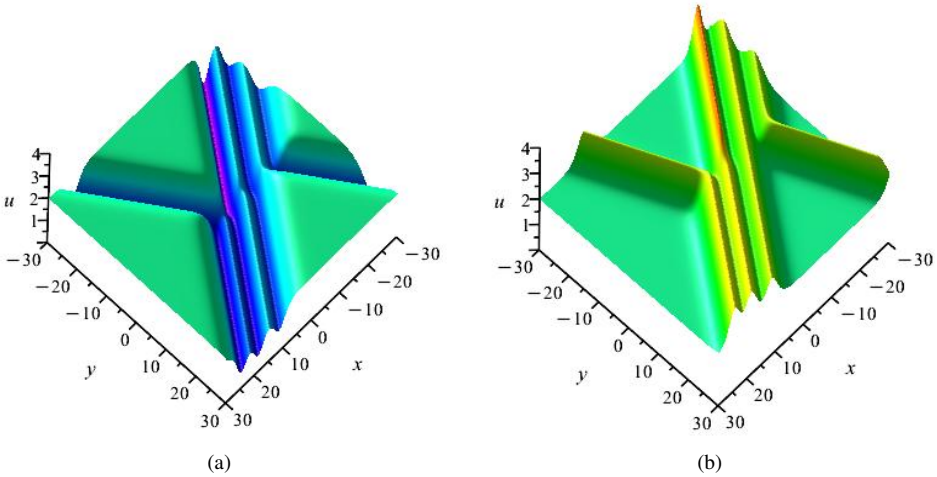


Fig. 11: (a) The dark 3-SMs-1-soliton solutions with the parameters chosen by $k_1 = -\frac{2}{3}, k_2 = -1, k_3 = -\frac{5}{6}, k_4 = -\frac{3}{4}, p_1 = \frac{1}{2}, p_2 = \frac{3}{4}, p_3 = \frac{5}{8}, p_4 = -\frac{1}{2}, q_1 = \frac{3}{4}, q_2 = \frac{211}{216}, q_3 = \frac{127}{144}, q_4 = 1, \alpha = \frac{1}{2}, \beta = -\frac{1}{3}, \gamma = \frac{2}{5}, \delta = \frac{3}{2}, \eta_1^0 = 0, \eta_2^0 = 0, \eta_3^0 = 0, \eta_4^0 = 0, z = 1, t = 0, C = 2$; (b) The anti-dark 3-SMs-1-soliton solutions with the parameters chosen by $k_1 = -\frac{2}{3}, k_2 = -1, k_3 = -\frac{5}{6}, k_4 = -\frac{3}{4}, p_1 = \frac{1}{2}, p_2 = \frac{3}{4}, p_3 = \frac{5}{8}, p_4 = -\frac{1}{3}, q_1 = \frac{3}{4}, q_2 = \frac{179}{216}, q_3 = \frac{119}{144}, q_4 = 1, \alpha = \frac{1}{2}, \beta = \frac{2}{3}, \gamma = \frac{4}{5}, \delta = \frac{3}{2}, \eta_1^0 = 0, \eta_2^0 = 0, \eta_3^0 = 0, \eta_4^0 = 0, z = 1, t = 0, C = 2$.

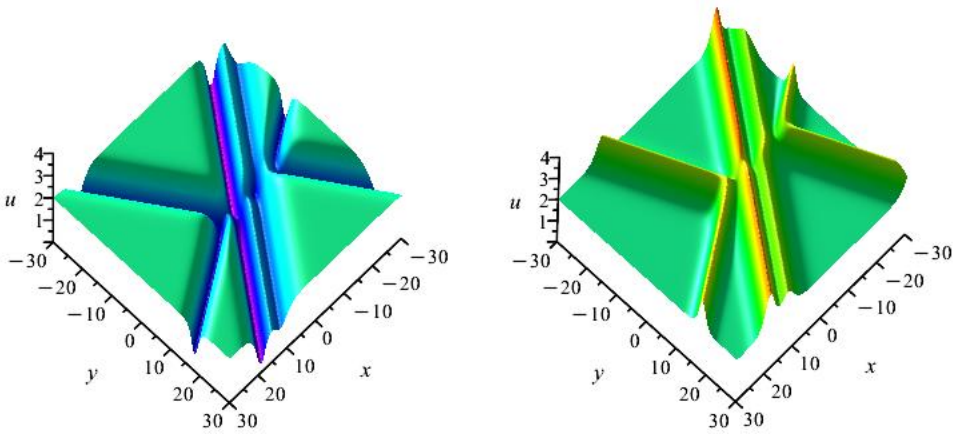


Fig. 12: (a) The dark 2-SMs-2-solitons solutions with the parameters chosen by $k_1 = -\frac{2}{3}$, $k_2 = -1$, $k_3 = -\frac{5}{6}$, $k_4 = -\frac{3}{4}$, $p_1 = \frac{1}{2}$, $p_2 = \frac{3}{4}$, $p_3 = \frac{4}{3}$, $p_4 = -\frac{1}{2}$, $q_1 = \frac{3}{4}$, $q_2 = \frac{211}{216}$, $q_3 = \frac{4}{5}$, $q_4 = 1$, $\alpha = \frac{1}{2}$, $\beta = -\frac{1}{3}$, $\gamma = \frac{2}{5}$, $\delta = \frac{3}{2}$, $\eta_1^0 = 0$, $\eta_2^0 = 0$, $\eta_3^0 = 0$, $\eta_4^0 = 0$, $z = 1$, $t = 0$, $C = 2$; (b) The anti-dark 2-SMs-2-solitons solutions with the parameters chosen by $k_1 = -\frac{2}{3}$, $k_2 = -1$, $k_3 = -\frac{5}{6}$, $k_4 = -\frac{3}{4}$, $p_1 = \frac{1}{2}$, $p_2 = \frac{3}{4}$, $p_3 = \frac{4}{3}$, $p_4 = -\frac{1}{3}$, $q_1 = \frac{3}{4}$, $q_2 = \frac{179}{216}$, $q_3 = \frac{4}{5}$, $q_4 = 1$, $\alpha = \frac{1}{2}$, $\beta = \frac{2}{3}$, $\gamma = \frac{4}{5}$, $\delta = \frac{3}{2}$, $\eta_1^0 = 0$, $\eta_2^0 = 0$, $\eta_3^0 = 0$, $\eta_4^0 = 0$, $z = 1$, $t = 0$, $C = 2$.

(3) Interactions of different dark SMs

In review of Eqs.(24) and (25), we consider N_1 solitons sharing the same velocity $V_{N_1,x}$, $V_{N_1,y}$, and N_2 solotions moving at another same velocity $V_{N_2,x}$, $V_{N_2,y}$, and thus can directly reduce the interaction between N_1-SMs and N_2-SMs ($2 \leq N_1, N_2 \leq N$) from the general SMs solutions (26). Here, we term this type of solution as N_1-SMs-N_2-SMs. By considering four solitons where two share an identical velocity $V_{1,x}, V_y$ and the remaining two share another common velocity $V_{2,x}, V_{2,y}$, where $V_{1,x} \neq V_{2,x}$ and $V_{1,y} \neq V_{2,y}$, we can obtain the 2-SMs-2-SMs solution, see Fig.13. As shown in Fig.13(a), the concave double stripes along the main diagonal correspond to the first dark 2-SMs, while those along the anti-diagonal correspond to the second dark 2-SMs. Their interaction gives rise to an X-shaped structure. Similarly, Fig.13(b) illustrates the anti-dark scenario. Similar to the four-soliton case, the collision between these two 2-SMs is also elastic. Both the velocities and amplitudes of the 2-SMs remain invariant before and after the collision, with only a phase shift occurring.

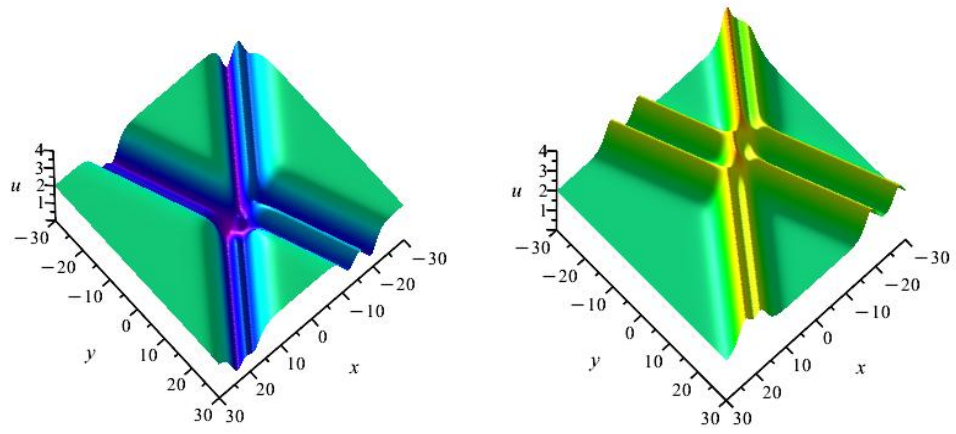


Fig. 13: (a) The dark 2-SMs-2-SMs solution with the parameters chosen by $k_1 = -\frac{2}{3}$, $k_2 = -1$, $k_3 = -\frac{5}{6}$, $k_4 = -\frac{3}{4}$, $p_1 = \frac{1}{2}$, $p_2 = \frac{3}{4}$, $p_3 = -\frac{1}{3}$, $p_4 = -\frac{3}{10}$, $q_1 = \frac{3}{4}$, $q_2 = \frac{211}{216}$, $q_3 = \frac{2}{5}$, $q_4 = \frac{9091}{3600}$, $\alpha = \frac{1}{2}$, $\beta = -\frac{1}{3}$, $\gamma = \frac{2}{5}$, $\delta = \frac{3}{2}$, $\eta_1^0 = 0$, $\eta_2^0 = 0$, $\eta_3^0 = 0$, $\eta_4^0 = 0$, $z = 1$, $t = 0$, $C = 2$; (b) the anti-dark 2-SMs-2-SMs solution with the parameters chosen by $k_1 = -\frac{2}{3}$, $k_2 = -1$, $k_3 = -\frac{5}{6}$, $k_4 = -\frac{3}{4}$, $p_1 = \frac{1}{2}$, $p_2 = \frac{3}{4}$, $p_3 = -\frac{1}{3}$, $p_4 = -\frac{3}{10}$, $q_1 = \frac{3}{4}$, $q_2 = \frac{179}{216}$, $q_3 = -\frac{4}{5}$, $q_4 = -\frac{1201}{1800}$, $\alpha = \frac{1}{2}$, $\beta = \frac{2}{3}$, $\gamma = \frac{4}{5}$, $\delta = \frac{3}{2}$, $\eta_1^0 = 0$, $\eta_2^0 = 0$, $\eta_3^0 = 0$, $\eta_4^0 = 0$, $z = 1$, $t = 0$, $C = 2$.

4. M-dark-lump solutions for the (3+1)-dimensional WKB equation

Unlike solitons, which are typically expressed in terms of hyperbolic functions and have a constant background, lump solutions are rationally localized in all spatial directions and decay algebraically to a constant background at infinity. Generally lumps can be primarily classified into two categories-bright and dark lumps. A bright lump is a type of positive-definite localized structure. It manifests as a localized “hump" or a peak protruding from a uniform, non-zero constant background. Conversely, a dark lump is characterized by a localized “dip" or a hole on a continuous wave background. Instead of a peak, it appears as a localized decrease in the amplitude of the background field. Visually, the density profile of a bright lump resembles an eye-shaped pattern, while that of a dark lump shows the inverse pattern. To the best of our knowledge, the dark lump solutions of Eq.(1) have not been reported; therefore, it is highly necessary and meaningful to investigate the lump solutions for this equation. In this section, we will derive M-dark-lump waves for Eq.(3) by introducing the complex conjugation and the long-wave limit methods in N-soliton solution (choosing N=2M) of Eq.(7).

To obtain M-lump solutions, we first introduce the long-wave limits and the complex conjugation conditions as follows

$$\begin{cases} k_1 = \rho K_1,\ k_2 = \rho K_2,\ k_3 = \rho K_3,\ \cdots,\ k_{2M} = \rho K_{2M}, \\ p_1 = \rho P_1,\ p_2 = \rho P_2,\ p_3 = \rho P_3,\ \cdots,\ p_{2M} = \rho P_{2M}, \\ q_1 = \rho Q_1,\ q_2 = \rho Q_2,\ q_3 = \rho Q_3,\ \cdots,\ q_{2M} = \rho Q_{2M}, \\ \rho \to 0. \end{cases} \tag{27}$$

and

$$\begin{cases} K_1 = K_2^*,\ K_3 = K_4^*,\ \cdots,\ K_{2M-1} = K_{2M}^*, \\ P_1 = P_2^*,\ P_3 = P_4^*,\ \cdots,\ P_{2M-1} = P_{2M}^*, \\ Q_1 = Q_2^*,\ Q_3 = Q_4^*,\ \cdots,\ Q_{2M-1} = Q_{2M}^*, \\ \eta_1^0 = \eta_2^0 = \eta_3^0 = \cdots = \eta_{2M}^0 = i\pi, \end{cases} \tag{28}$$

where $K_i,\ P_i,\ Q_i$ ($1 \le i \le 2M$) are all arbitrary complex constants, ρ is an infinitesimal and the symbol “$*$" refers to the complex conjugate. Performing the above-mentioned two operations on Eq.(7) yields the concrete expressions of M-dark-lump solutions

$$\begin{cases} u = \dfrac{6\gamma}{\beta}(\ln f_{2M}^{'})_{xx} + C, \\ f_{2M}^{'} = \lim\limits_{\rho\to 0} \dfrac{1}{\rho^M}\Big(\sum\limits_{\mu=0,1} \exp\big(\sum\limits_{i=1}^{N} \mu_i\eta_i + \sum\limits_{1\le i<j}^{N} \mu_i\mu_j A_{ij}\big)\Big). \end{cases} \tag{29}$$

Choosing M=1 in Eq.(29), the concrete expressions of one-dark-lump solution admit

$$u = \frac{6\gamma}{\beta}\Big(\ln\left(\Theta_1\Theta_2 + \zeta_{12}\right)\Big)_{xx} + C, \tag{30}$$

with

$$\begin{aligned} \Theta_1 &= -\frac{tP_1\alpha}{2} + t\sqrt{(1+2C\beta)K_1^2 - \delta K_1 Q_1} + K_1 x + P_1 y + Q_1 z, \\ \Theta_2 &= -\frac{tP_2\alpha}{2} + t\sqrt{(1+2C\beta)K_2^2 - \delta K_2 Q_2} + K_2 x + P_2 y + Q_2 z, \\ \zeta_{12} &= \frac{12K_1^2K_2^2\gamma}{2\sqrt{K_1K_2((1+2C\beta)K_1 - \delta Q_1)((1+2C\beta)K_2 - \delta Q_2)} + \delta(K_1Q_2 + K_2Q_1) - (2+4C\beta)K_1K_2}. \end{aligned}$$

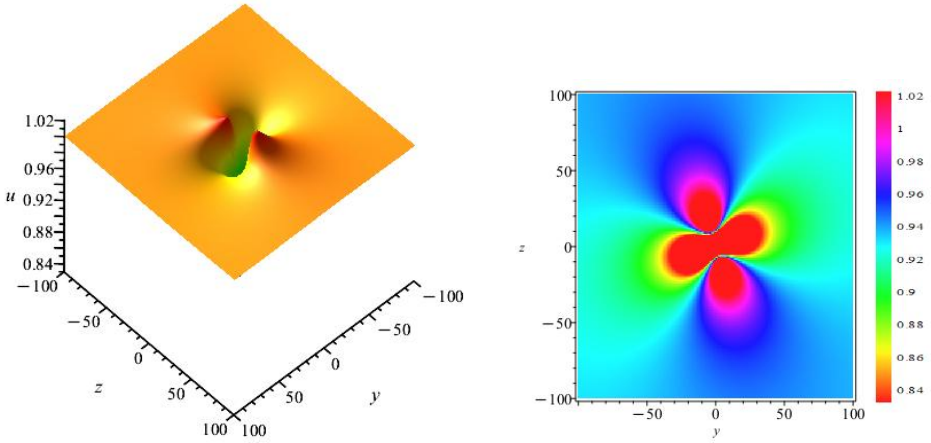
In review of the above terms, non-singular condition for the solution requirers that

$$\begin{cases} (1+2C\beta)K_1^2 - \delta K_1 Q_1 > 0, \\ 2\sqrt{K_1K_2((1+2C\beta)K_1 - \delta Q_1)((1+2C\beta)K_2 - \delta Q_2)} + \delta(K_1Q_2 + K_2Q_1) - (2+4C\beta)K_1K_2 \neq 0. \end{cases}$$

Analogous to the case of bright and dark solitons in Sec.2, the types of bright and dark lumps here are also simultaneously governed by theses two parameters γ and β. For γ>0 and β<0, with the remaining free parameters

in Eq.(30) specified in the caption of Fig.14, the concrete expression for one-dark-lump solution can be given as

$$u = \frac{1152(\sqrt{178}-13)(\sqrt{178}(y-\frac{z}{2}+1)(y+2z-2)-13y^2+(13-\frac{39z}{2})y+13z^2-39z+\frac{274}{5})}{125(\sqrt{178}(y^2+z^2+\frac{4y}{5}-\frac{12z}{5}+\frac{8}{5})-13y^2-13z^2-\frac{52y}{5}+\frac{156z}{5}+\frac{56}{25})^2}. \tag{31}$$



(a) (b)

Fig. 14: One-dark-lump solution with the parameters chosen by $K_1 = K_2^* = -1+i$, $P_1 = P_2^* = \frac{1}{2}+i$, $Q_1 = Q_2^* = 1-\frac{i}{2}$, $\alpha = \frac{1}{2}$, $\beta = -\frac{1}{3}$, $\gamma = \frac{1}{5}$, $\delta = 1$, $x = 1$, $t = 0$, $C = 1$.

In Fig.14(a), it obviously shows two maxima located above the nonzero constant background and one minimum below, which is opposite to the typical bright lump structure, thus identifying it as a dark lump wave. Furthermore, Fig.14(b) displays a distinct inverse eye-shaped structure, which further corroborates that the lump identified here is indeed a dark one.

Similar to the one-lump solution, the two-dark-lump solutions corresponds to the choice of M= 2 in Eq.(29), i.e.,

$$\begin{cases} u = \dfrac{6\gamma}{\beta}(\ln f_4')_{xx} + C, \\ f_4' = \Theta_1\Theta_2\Theta_3\Theta_4 + \zeta_{12}\Theta_3\Theta_4 + \zeta_{13}\Theta_2\Theta_4 + \zeta_{14}\Theta_2\Theta_3 + \zeta_{23}\Theta_1\Theta_4 \\ \quad +\zeta_{24}\Theta_1\Theta_3 + \zeta_{34}\Theta_1\Theta_2 + \zeta_{12}\zeta_{34} + \zeta_{13}\zeta_{24} + \zeta_{14}\zeta_{23}, \end{cases} \tag{32}$$

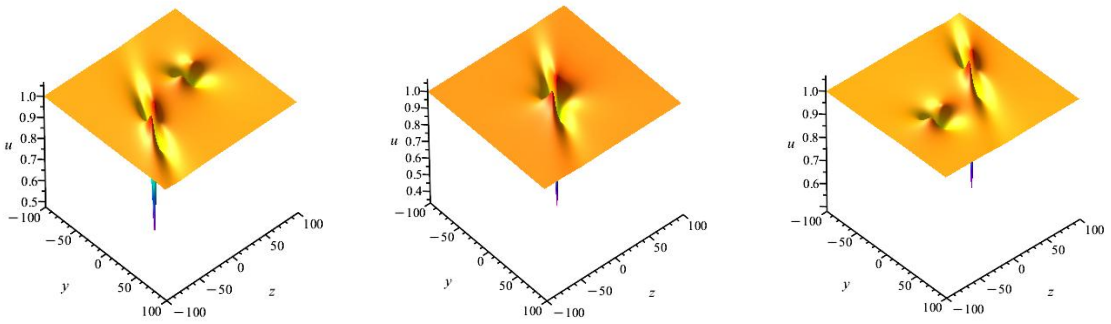
where

$$\begin{aligned} \Theta_i &= -\frac{tP_i\alpha}{2} + t\sqrt{(1+2C\beta)K_i^2 - \delta K_iQ_i} + K_ix + P_iy + Q_iz \ (i = 1,2,3,4), \\ \zeta_{ij} &= \frac{12K_i^2K_j^2\gamma}{2\sqrt{K_iK_j((1+2C\beta)K_i - \delta Q_i)((1+2C\beta)K_j - \delta Q_j)} + \delta(K_iQ_j + K_jQ_i) - (2+4C\beta)K_iK_j} (1\le i<j\le 4). \end{aligned} \tag{33}$$

Here, the non-singularity conditions for the two-dark-lump solutions are given by

$$\begin{cases} (1+2C\beta)K_i^2 - \delta K_iQ_i > 0, \\ 2\sqrt{K_iK_j((1+2C\beta)K_i - \delta Q_i)((1+2C\beta)K_j - \delta Q_j)} + \delta(K_iQ_j + K_jQ_i) - (2+4C\beta)K_iK_j \neq 0. \end{cases}$$

As shown in Fig.15(a) (t=−30), one can easily observe that two dark lump waves on the nonzero background plane. Specifically, the one in the lower left exhibits a higher amplitude, whereas the one in the upper right has a relatively lower amplitude. At t=0, these two lump waves undergo a significant interaction, culminating in their mutual fusion, see Fig.15(b). At t=30, the lump wave with the higher amplitude overtakes the one with the lower amplitude. Subsequently, they preserve their respective shapes and speeds, continuing to propagate along their original trajectories. Since the entire interaction process of the 2-lump solution bears a striking resemblance to that of 2-soliton, the collisions of multi-lump solutions are also elastic.



(a) (b) (c)

Fig. 15: Two-dark-lump solutions with the parameters chosen by $K_1 = K_2^* = -1 + i$, $K_3 = K_4^* = \frac{1}{2} - \frac{3i}{2}$, $P_1 = P_2^* = \frac{1}{2} + i$, $P_3 = P_4^* = \frac{3}{4} + i$, $Q_1 = Q_2^* = 1 - \frac{i}{2}$, $Q_3 = Q_4^* = \frac{1}{5} + 2i$, $\alpha = \frac{1}{2}, \beta = -\frac{1}{3}, \gamma = \frac{1}{5}, \delta = 1, x = 1, C = 1$: (a) $t = -30$; (b) $t = 0$; (c) $t = 30$.

5. The dark interactional solutions for the (3+1)-dimensional WKB equation

In previous sections, we have derived several types of dark localized wave solutions of Eq.(1), such as dark solitons, resonant solitons and lumps. To elucidate the dynamics of the dark localized waves obtained above, we systematically investigate the interactions among four distinct species: dark solitons, dark-resonant-Y-shaped-soliton, dark breathers, and dark lumps. Utilizing the complex conjugation and the long-wave limit methods, we will mainly discuss these three different interactional solutions: (1) multi dark resonant Y-shaped solitons and mutli-solitons; (2) multi dark lumps and multi-solitons; (3) multi dark breathers and lumps. For the sake of discussion, we present only a few representative examples of the above-mentioned hybrid solutions.

(1) Interactions between M-dark-resonant-Y-shaped-soliton and $(N-2M)$-soliton

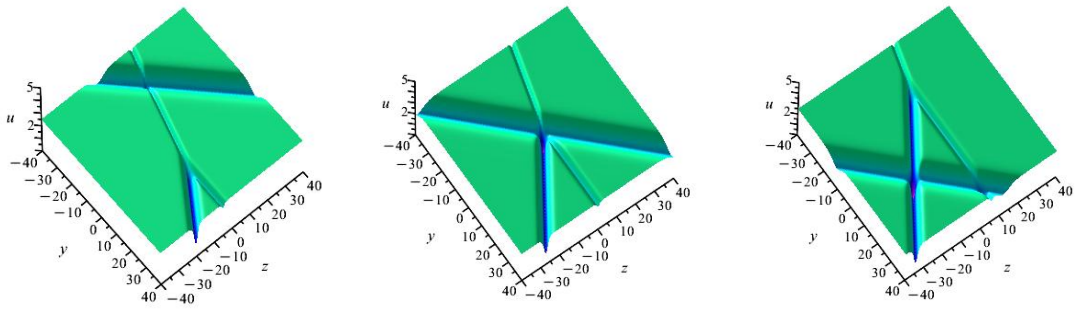
By selecting $2M$ solitons to undergo resonance while leaving the remaining $(N-2M)$ as standard solitons in Eq.(7), we can derive the interaction solutions featuring M Y-shaped solitons and $(N-2M)$-soliton. Referring to Eqs.(17) and (7), we can obtain the interactional solution between M-dark-resonant-Y-shaped-soliton and $(N-2M)$-soliton as $(1 \le M < [\frac{N}{2}])$

$$\begin{cases} u = \dfrac{6\gamma}{\beta}\Big(\ln\Big(\sum\limits_{\mu=0,1}\exp\big(\sum\limits_{i=1}^{N}\mu_i\eta_i + \sum\limits_{1\le i<j}^{N}\mu_i\mu_j A_{ij}\big)\Big)\Big)_{xx} + C, \\ q_{2m} = \dfrac{2\gamma k_{2m}(k_{2m-1}^2 - 3k_{2m-1}k_{2m} + 2k_{2m}^2)}{\delta} + \dfrac{k_{2m}q_{2m-1}}{k_{2m-1}} \\ \quad - \dfrac{2k_{2m}\sqrt{-3\gamma k_{2m-1}^3(k_{2m-1}-k_{2m})^2(\gamma k_{2m-1}^3 + 2C\beta k_{2m-1} - \delta q_{2m-1} + k_{2m-1})}}{k_{2m-1}^2\delta} \ (1 \le m \le M), \end{cases} \tag{34}$$

where the values of η_i and $e^{A_{ij}}$ have been given in Eqs.(8)-(8), and the restriction imposed on the parameters to avoid singularity of u is

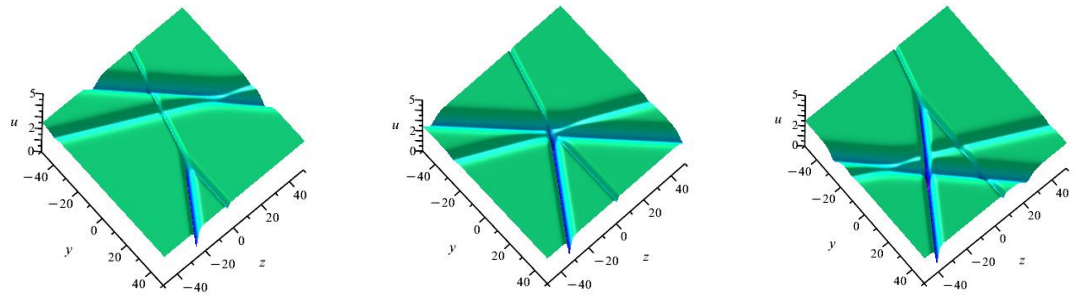
$$\gamma k_{2m-1}^3(\gamma k_{2m-1}^3 + 2C\beta k_{2m-1} - \delta q_{2m-1} + k_{2m-1}) < 0.$$

Choosing N=3, M=1 in Eq.(34), the interactions between one-Y-shaped-soliton and one-soliton can be shown in Fig.16. As illustrated in the evolution process from Fig.16 (a) to (c), the dark Y-shaped soliton propagates from the lower-left to the upper-right, whereas the standard dark soliton moves in the opposite direction. Notably, a significant collision occurs at the bifurcation point of the Y-shaped structure at t=0. Furthermore, both the amplitudes and velocities remain invariant for each wave after the collision, with only a phase shift observed. It unequivocally demonstrates the elastic nature of the interaction between the Y-shaped soliton and the standard dark soliton. To verify the heredity of these interaction solutions, we similarly present an interaction scenario involving one Y-shaped soliton and two standard solitons by setting N=4, M=2 in Eq.(34), see Fig.17. Analogous to the evolution depicted in Fig.16, the interaction between the Y-shaped soliton and the two solitons in Fig.17 is also perfectly elastic.



(a) (b) (c)

Fig. 16: Interactions between one-dark-resonant-Y-shaped-soliton and one-soliton with the parameters chosen by $k_1 = 1$, $k_2 = \frac{1}{2}$, $k_3 = -\frac{2}{3}$, $p_1 = 1$, $p_2 = 1$, $p_3 = -\frac{1}{2}$, $q_1 = \frac{3}{2}$, $q_2 = \frac{3+3\sqrt{15}}{4}$, $q_3 = \frac{1}{2}$, $\alpha = 1, \beta = \frac{1}{2}$, $\gamma = -\frac{1}{2}$, $\delta = \frac{1}{3}$, $\eta_1^0 = 0$, $\eta_2^0 = 0$, $\eta_3^0 = 0$, $x = 1$, $C = \frac{5}{2}$: (a) $t = -10$; (b) $t = 0$; (c) $t = 10$.



(a) (b) (c)

Fig. 17: Interactions between one-dark-resonant-Y-shaped-soliton and two-soliton with the parameters selected being the same as those in Fig.(16) except $k_4 = -\frac{1}{3}$, $p_4 = -\frac{2}{3}$, $q_4 = \frac{1}{3}$, $\eta_4^0 = 0$: (a) $t = -10$; (b) $t = 0$; (c) $t = 10$.

(2) Interactions between M-dark-lump solutions and $(N-2M)$-soliton

In review of Eq.(7) and Eq.(29), we can derive the interactions of M-dark-lump and $(N-2M)$-soliton by choosing $2M$ solitons to constitute M-lump waves, the other $(N-2M)$ solitons are kept unchanged ($1 \leq M < [\frac{N}{2}]$). Owing to the prohibitive complexity of the general expression for this kind of interactional solution, we refrain from presenting its arbitrary form and instead provide explicit expressions only for two specific instances: one lump wave interacting with one-soliton and two-soliton state.

Setting $N=3$, $M=1$ in Eqs.(7) and (29), we first introduce the following constraints to successfully derive one-lump

$$\begin{cases} k_1 = \rho K_1,\ k_2 = \rho K_2,\ p_1 = \rho P_1,\ p_2 = \rho P_2,\ q_1 = \rho Q_1,\ q_2 = \rho Q_2, \\ \eta_1^0 = \eta_2^0 = i\pi,\ K_1 = K_2^*,\ P_1 = P_2^*,\ Q_1 = Q_2^*, \\ \rho \to 0, \end{cases} \tag{35}$$

where K_j, P_j, Q_j $(j=1,2)$ are all arbitrary complex constants. Substituting Eq.(35) to Eq.(7), one can give the concrete expression of the interactional solution that one-dark-lump and one-dark-soliton as

$$\begin{cases} u = \dfrac{6\gamma}{\beta}(\ln f_3'')_{xx} + C, \\ f_3'' = \Theta_1\Theta_2 + \zeta_{12} + e^{\eta_3}(\Theta_1\Theta_2 + \zeta_{12} + \Theta_1\Omega_{23} + \Theta_2\Omega_{13} + \Omega_{13}\Omega_{23}), \end{cases} \tag{36}$$

with

$$\Omega_{13}=\frac{12K_1^2k_3^2\gamma}{2\sqrt{K_1k_3((1+2C\beta)K_1-\delta Q_1)(\gamma k_3^3+(1+2C\beta)k_3)-\delta q_3}+\delta(K_1q_3+k_3Q_1)-4\gamma K_1k_3^3-(4C\beta+2)K_1k_3},$$

$$\Omega_{23}=\frac{12K_2^2k_3^2\gamma}{2\sqrt{K_2k_3((1+2C\beta)K_2-\delta Q_2)(\gamma k_3^3+(1+2C\beta)k_3)-\delta q_3}+\delta(K_2q_3+k_3Q_2)-4\gamma K_2k_3^3-(4C\beta+2)K_2k_3},$$

$$\omega_3=-\frac{p_3\alpha}{2}+\sqrt{k_3^4\gamma-k_3q_3\delta+(1+2C\beta)k_3^2},\ \eta_3=\omega_3t+k_3x+p_3y+q_3z+\eta_3^0,$$

where $\Theta_1,\ \Theta_2$ and ζ_{12} have been given in Eq.(33).

By the same token, we can directly construct the interactional solutions between one-lump and two solitons by choosing N=3, M=1 in Eqs.(7) and (29), i.e.,

$$\begin{cases} u=\dfrac{6\gamma}{\beta}(\ln f_4'')_{xx}+C, \\ f_4''=\Theta_1\Theta_2+\zeta_{12}+e^{\eta_3}(\Theta_1\Theta_2+\zeta_{12}+\Theta_1\Omega_{23}+\Theta_2\Omega_{13}+\Omega_{13}\Omega_{23}) \\ +e^{\eta_4}(\Theta_1\Theta_2+\zeta_{12}+\Theta_1\Omega_{24}+\Theta_2\Omega_{14}+\Omega_{14}\Omega_{24})+e^{\eta_3}e^{\eta_4}e^{A_{34}}(\Theta_1\Theta_2 \\ +\zeta_{12}+\Theta_1\Omega_{23}+\Theta_1\Omega_{24}+\Theta_2\Omega_{13}+\Theta_2\Omega_{24}+\Omega_{13}\Omega_{23} \\ +\Omega_{13}\Omega_{24}+\Omega_{14}\Omega_{23}+\Omega_{14}\Omega_{24}), \end{cases} \tag{37}$$

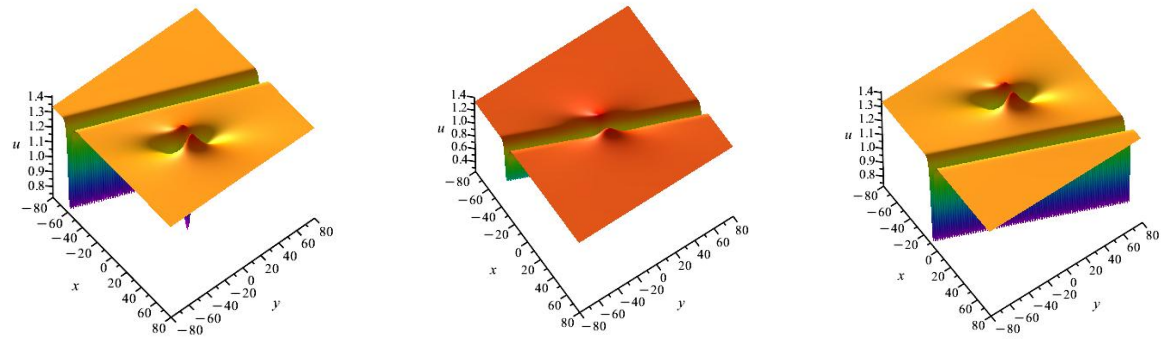
with

$$\Omega_{ij}=\frac{12K_i^2k_j^2\gamma}{2\sqrt{K_ik_j((1+2C\beta)K_i-\delta Q_i)(\gamma k_j^3+(1+2C\beta)k_j)-\delta q_j}+\delta(K_iq_j+k_jQ_i)-4\gamma K_ik_j^3-(4C\beta+2)K_ik_j},$$

$$\omega_j=-\frac{p_j\alpha}{2}+\sqrt{k_j^4\gamma-k_jq_j\delta+(1+2C\beta)k_j^2},\ \eta_j=\omega_jt+k_jx+p_jy+q_jz+\eta_j^0\ (i=1,2,j=3,4),$$

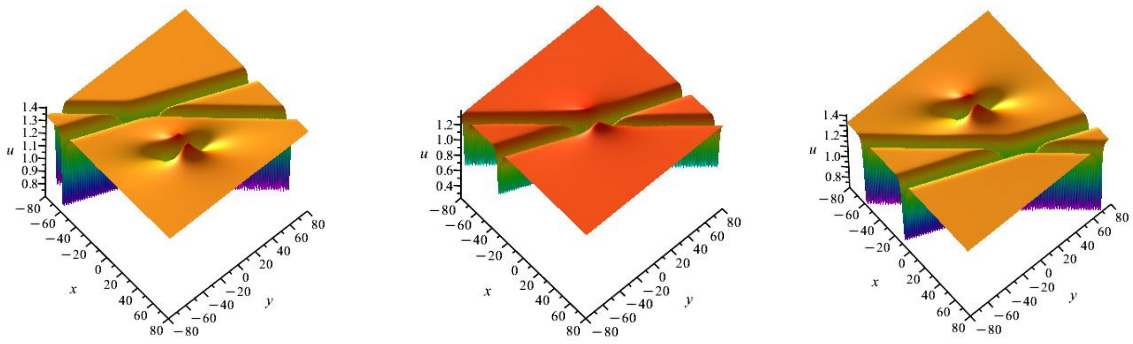
where $e^{A_{34}}$, $\Theta_1,\ \Theta_2$ and ζ_{12} have been given in Eq.(10) and Eq.(33).

For the one-dark-lump wave derived above, its interactions with one-dark-soliton and with two-dark-soliton are illustrated in Fig.18 and Fig.19, respectively. At $t=-20$ (Fig.18(a)), the anti-eye-shaped single dark lump wave is positioned below the nonzero background plane, while the single dark soliton resides above it. Over time, the lump wave propagates upward toward the nonzero background plane, while the dark soliton moves downward. At t=0, they undergo a significant interaction, during which the lump effectively sinks into the dip of the dark soliton, see Fig.18(b). As shown in Fig.18(c) ($t=-20$), the two structures exchange positions, with the lump emerging above the soliton. Thereafter, they resume propagation along their respective trajectories, fully retaining their original amplitudes and velocities. Based on the interaction dynamics described above, the collision between the lump wave and the dark soliton is elastic, closely resembling that of multi-soliton interactions. Analogously, the interaction between the single lump wave and the two-soliton system also constitutes an elastic collision, as specifically illustrated in Fig.19.



(a) (b) (c)

Fig. 18: Interactions with one-dark-lump and one-dark-soliton with the parameters chosen by $K_1=K_2^*=\frac{1}{2}-\frac{3}{2}i$, $k_3=-\frac{4}{5}$, $P_1=P_2^*=\frac{3}{4}+i$, $p_3=\frac{1}{3}$, $Q_1=Q_2^*=\frac{1}{5}+2i$, $q_3=\frac{4}{3}$, $\alpha=\frac{1}{2}$, $\beta=-\frac{1}{3}$, $\gamma=\frac{1}{5}$, $\delta=1$, $\eta_3^0=0$, $z=1$, $C=\frac{4}{3}$: (a) $t=-20$; (b) $t=0$; (c) $t=20$.



(a) (b) (c)

Fig. 19: Interactions between one-dark-lump and two-dark-soliton with the parameters selected being the same as those in Fig.(18) and $k_4 = -\frac{5}{6}$, $p_4 = \frac{3}{4}$, $q_4 = \frac{4}{5}$, $\eta_4^0 = 0$: (a) $t = -20$; (b) $t = 0$; (c) $t = 20$.

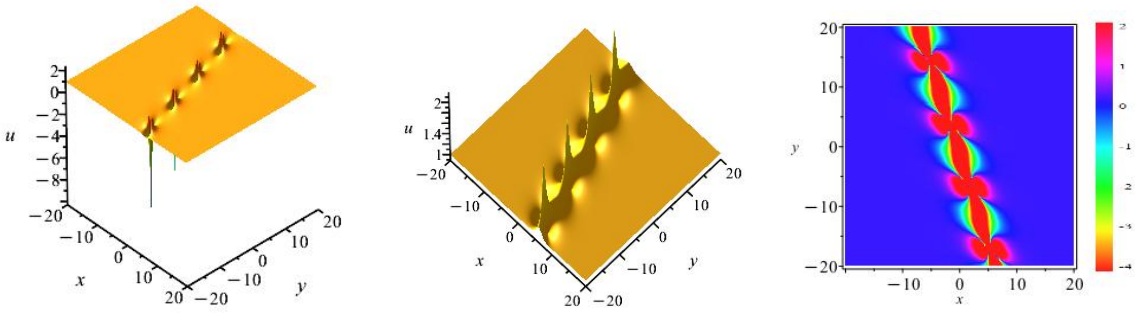
(3) Interactions between M_1-dark-lump solutions and M_2-dark-breather

As discussed in Sec.4, to facilitate the derivation of both lump waves and breathers, we must set N to be an even number in Eq.(7). Choosing $2M_1$ solitons to constitute M_1-lump waves, $2M_2$ solitons to generate M_2-breather, one can get the interactional solution that between M_1-dark-lump and M_2-dark-breather (M_1+M_2=N).

When N=2, M_1=1, one can get one-breather solution by introducing the following complex conjugate constraints in Eq.(7)

$$k_1 = k_2^*,\ p_1 = p_2^*,\ q_1 = q_2^*. \tag{38}$$

Similar to the lump solutions, the classification of bright and dark one-breather is likewise dictated by parameters γ and β, see Fig.20. As shown in Fig.20(a), the amplitude on the nonzero background plane is smaller than that beneath it; such a structure is referred to as a dark breather. Conversely, Fig.20(b) displays the opposite scenario, corresponding to a standard breather. Furthermore, Fig.20(c) presents a periodic anti-eye-shaped structure, which further corroborates? the characteristic profile of the dark breather.



(a) (b) (c)

Fig. 20: Two types of one-breather with the parameters chosen by $k_1 = k_2^* = 1 + \frac{i}{5}$, $p_1 = p_2^* = \frac{1}{3} + \frac{2}{3}i$, $q_1 = q_2^* = \frac{1}{2} + i$, $\alpha = -\frac{1}{2}$, $\gamma = \frac{1}{10}$, $\delta = 5$, $\eta_1^0 = 0$, $\eta_2^0 = 0$, $z = 1$, $C = 1$, $t = 0$:(a) one-dark-breather ($\beta = -3$); (b) normal one-breather ($\beta = 3$);(c) the density plot of one-dark-breather.

Choosing M_1=M_2=1 in Eq.(7), one can derive the interactional solution between one-dark-lump and one-dark-breather by introducing the following complex conjugate and long-wave limit constraints

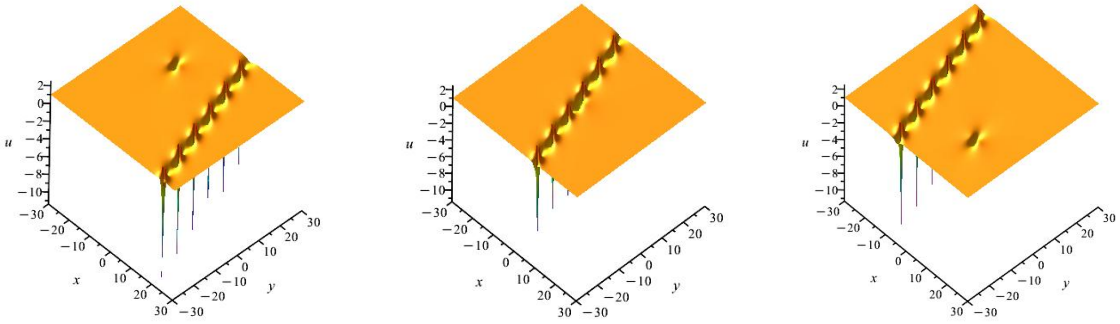
$$\begin{cases} k_1 = \rho K_1,\ k_2 = \rho K_2,\ p_1 = \rho P_1,\ p_2 = \rho P_2,\ q_1 = \rho Q_1,\ q_2 = \rho Q_2, \\ k_3 = k_4^*,\ p_3 = p_4^*,\ q_3 = q_4^*, \\ \eta_1^0 = \eta_2^0 = i\pi,\ K_1 = K_2^*,\ P_1 = P_2^*,\ Q_1 = Q_2^*, \\ \rho \to 0, \end{cases} \tag{39}$$

where K_j, P_j, Q_j (j=1, 2) are all arbitrary complex constants. Employing Eq.(39) to Eq.(7), we can get the

expressions of the hybrid solution of one-dark-lump and one-dark-breather as

$$\begin{cases} u = \dfrac{6\gamma}{\beta}(\ln f_4''')_{xx} + C, \\ f_4''' = \Theta_1\Theta_2 + \zeta_{12} + e^{\eta_3}(\Theta_1\Theta_2 + \zeta_{12} + \Theta_1\Omega_{23} + \Theta_2\Omega_{13} + \Omega_{13}\Omega_{23}) \\ +e^{\eta_4}(\Theta_1\Theta_2 + \zeta_{12} + \Theta_1\Omega_{24} + \Theta_2\Omega_{14} + \Omega_{14}\Omega_{24}) + e^{\eta_3}e^{\eta_4}e^{A_{34}} \\ (\Theta_1\Theta_2 + \zeta_{12} + \Theta_1\Omega_{23} + \Theta_1\Omega_{24} + \Theta_2\Omega_{13} + \Theta_2\Omega_{24} + \Omega_{13}\Omega_{23} \\ +\Omega_{13}\Omega_{24} + \Omega_{14}\Omega_{23} + \Omega_{14}\Omega_{24}), \end{cases} \tag{40}$$

where ω_j, $e^{A_{34}}$, Θ_1, Θ_2, ζ_{12} and Ω_{ij} have been given in Eqs.(10) and (33). As depicted in Fig.21, the breather propagates from the lower right to the upper left of the non-zero plane, while the lump wave travels in the opposite direction, from the upper left to the lower right. Moving toward each other, the two structures merge into one at t=0 before separating again. From Fig.21(a) to (c), the interactions between this one-breather and one-lump wave consistently exhibit behavior analogous to that of multi-soliton, leaving no doubt that these collision is elastic.



(a) (b) (c)

Fig. 21: Interactions between one-dark-lump and one-dark-breather with the parameters chosen by $K_1 = K_2^* = -1 + i$, $k_3 = k_4^* = 1 + \frac{i}{5}$, $P_1 = P_2^* = \frac{1}{2} + i$, $p_3 = p_4^* = \frac{1}{3} + \frac{2}{3}i$, $Q_1 = Q_2^* = 1 - \frac{i}{2}$, $q_3 = q_4^* = \frac{1}{2} + i$, $\alpha = -\frac{1}{2}$, $\beta = -2$, $\gamma = \frac{1}{5}$, $\delta = 5$, $\eta_3^0 = 0$, $\eta_4^0 = 0$, $z = 1$, $C = 1$: (a) $t = -10$; (b) $t = 0$; (c) $t = 10$.

6. Conclusion and discussion

Beginning from the nonzero background, three kinds of dark localized waves-dark resonant solitons, the general dark SMs, and dark lumps-are systematacially investigated in Eq.(1), along with their interactions. Introducing a nonzero constant C in the variable transformation, the general dark resonant solitons, including Y-shaped and X-shaped solitons, are successfully reduced from the received N-dark-soliton. Introducing the velocity resonant conditions in the received N-soliton, one can derive the general dark SMs, which can be classified into three categories: pure dark SMs, dark SMs interacting with standard dark solitons, and hybrid solutions of different dark SMs. Besides, the general expression for M-lump solutions is derived by employing the complex conjugate and long-wave limit methods. Finally, three types of different interactional solutions are mainly given: (1) multi dark resonant Y-shaped solitons and mutli-solitons; (2) multi dark lumps and multi-solitons; (3) multi dark breathers and lumps. In light of the diverse potential applications of these three classes of dark localized waves, we look forward to their experimental verification in future physical setups.

Acknowledgement

This work is supported by National Natural Science Foundation of China (Grant No.12201578), Natural Science Foundation of Henan Province (Grant Nos.262300420708, 222300420377), Educational Commission of Henan Province of China (Grant No.25A110004), the Doctor Scientific Research Fund of Zhengzhou University of Light Industry and the Youth Core Teachers Foundation of Zhengzhou University of Light Industry.

Conflict of interest

All persons who have made substantial contributions to the work reported in the manuscript are named. The authors declare that there is no conflict of interests regarding the publication of this paper.

Author contributions

Tao Xu: Funding acquisition (lead), Methodology (lead), Supervision (equal), Software (equal), Writing-original draft (equal), Writing-review & editing (equal); Haiqing Zhang: Software (equal), Writing-original draft (equal); Abdul-Majid Wazwaz: Writing-review&editing (equal), Supervision (equal); Yaonan Shan: Funding acquisition (equal), Writing-review & editing (equal).

Data availability

No data was used for the research described in the article.

References

References

[1] S. Kumar, B. Mohan, R. Kumar, Lump, soliton, and interaction solutions to a generalized two-mode higher-order nonlinear evolution equation in plasma physics, Nonlinear Dynam. 110 (2022) 693-704.
[2] A. I. Maimistov, Solitons in nonlinear optics, Quantum Electron. 40 (2010) 756.
[3] M. Tlidi, M. Taki, Rogue waves in nonlinear optics, Adv. Optics Photonics 14 (2022) 87-147.
[4] J. Kalita, R. Das, K. Hosseini, D. Baleanu, S. Salahshour, Solitons in magnetized plasma with electron inertia under weakly relativistic effect, Nonlinear Dynam. 111 (2023) 3701-3711.
[5] G. Q. Xu, A. M. Wazwaz, Characteristics of integrability, bidirectional solitons and localized solutions for a (3+1)-dimensional generalized breaking soliton equation, Nonlinear Dynam. 96 (2019) 1989-2000.
[6] Y. H. Yin, X. L??, W. X. Ma, Bäcklund transformation, exact solutions and diverse interaction phenomena to a (3+1)-dimensional nonlinear evolution equation, Nonlinear Dynam. 108 (2022) 4181-4194.
[7] W. X. Ma, Y. J. Zhang, Darboux transformations of integrable couplings and applications, Rev. Math. Phys. 30 (2018) 1850003.
[8] L. M. Ling, L. C. Zhao, B. L. Guo, Darboux transformation and multi-dark soliton for N-component nonlinear Schrödinger equations, Nonlinearity 28 (2015) 3243-3261.
[9] T. Xu, Y. Wang, Y. N. Shan, Soliton molecules and breather-positon solutions in the Heisenberg ferromagnet-type of Akbota equation, Phys. Scr. 100 (2025) 075212.
[10] M. R. Ali, M. A. Khattab, S. M. Mabrouk, Optical soliton solutions for the integrable Lakshmanan-Porsezian-Daniel equation via the inverse scattering transformation method with applications, Optik 272 (2022) 170256.
[11] W. X. Ma, Y. Zhang, Y. N. Tang, J. Y. Tu, Hirota bilinear equations with linear subspaces of solutions, Appl. Math. Comput. 218 (2012) 7174-7183.
[12] L. Li, C. N. Duan, F. J. Yu, An improved Hirota bilinear method and new application for a nonlocal integrable complex modified Korteweg-de Vries (MKdV) equation, Phys. Lett. A 383 (2019) 1578-1582.
[13] R. F. Zhang, S. Bilige, Bilinear neural network method to obtain the exact analytical solutions of nonlinear partial differential equations and its application to p-gBKP equation, Nonlinear Dynam. 95 (2019) 3041-3048.
[14] R. F. Zhang, M. C. Li, J. Y. Gan, Q. Li, Z. Z. Lan, Novel trial functions and rogue waves of generalized breaking soliton equation via bilinear neural network method, Chaos Soliton Fract. 154 (2022) 111692.
[15] W. X. Ma, Riemann-Hilbert problems and inverse scattering of nonlocal real reverse-spacetime matrix AKNS hierarchies, Physica D 430 (2022) 133078.
[16] B. J. Wang, Z. M. Ma, S. H. Xiong, M-lump, rogue waves, breather waves, and interaction solutions among four nonlinear waves to new (3+1)-dimensional Hirota bilinear equation, Nonlinear Dynam. 111 (2023) 9477-9494.
[17] Y. Shen, B. Tian, C. D. Cheng, T. Y. Zhou, N-soliton, Mth-order breather, Hth-order lump, and hybrid solutions of an extended (3+1)-dimensional Kadomtsev-Petviashvili equation, Nonlinear Dynam. 111 (2023) 10407-10424.
[18] Z. L. Zhao, L. C. He, Multiple lump solutions of the (3+1)-dimensional potential Yu-Toda-Sasa-Fukuyama equation, Appl. Math. Lett. 95 (2019) 114-121.
[19] Z. M. Ma, B. H. Chen, Q. M. Bi, Multiple rogue wave solutions for a modified (2+1)-dimensional nonlinear evolution equation, Nonlinear Dynam. 112 (2024) 20141-20151.
[20] Ohta Y, D. S. Wang, J. K. Yang, General N-Dark-Dark solitons in the coupled nonlinear Schrödinger equations, Stud. Appl. Math. 127 (2009) 345-371.
[21] L. M. Ling, L. C. Zhao, B. L. Guo, Darboux transformation and multi-dark soliton for N-component nonlinear Schrödinger equations, Nonlinearity 28 (2015) 3243-3261.
[22] S. Burger, K. Bongs, S. Dettmer, W. Ertmer, K. Sengstock, A. Sanpera, G. V. Shlyapnikov, M. Lewenstein, Dark solitons in Bose-Einstein condensates, Phys. Rev. Lett. 83 (1999) 5198-5201.
[23] J. G. Rao, D. Mihalache, F. Zhou, J. S. He, S. A. Chen, Dark and antidark solitons on continuous and doubly periodic backgrounds in the space-shifted nonlocal nonlinear Schrödinger equation, Chaos Solitons Fractals 182 (2024) 114846.
[24] G. X. Zhang, C. Y. Shi, C. F. Wu, B. F. Feng, Dark soliton and breather solutions to the coupled Sasa-Satsuma equation, J. Nonlinear Sci. 35 (2025) 7.
[25] L. M. Ling, X. Sun, Multi-elliptic-dark soliton solutions of the defocusing nonlinear Schrödinger equation, Appl. Math. Lett. 148 (2024) 108866.
[26] X. Wang, J. S. He, Dark solitons on elliptic function background for the defocusing Hirota equation, Commun. Theor. Phys. 77 (2025) 035003.

[27] X. Wang, Z. Y. Yan, X. Y. Yang, The defocusing Lakshmanan-Porsezian-Daniel equation with elliptic function backgrounds: N-elliptic-dark solitons and asymptotic behaviors, Appl. Math. Lett. 171 (2025) 109684.
[28] Y. L. Ma, A. M. Wazwaz, B. Q. Li, Soliton resonances, soliton molecules, soliton oscillations and heterotypic solitons for the nonlinear Maccari system, Nonlinear Dyn. 111 (2023) 18331-18344.
[29] K. J. Wang, Resonant Y-type soliton, X-type soliton and some novel hybrid interaction solutions to the (3+1)-dimensional nonlinear evolution equation forshallow-water waves, Phys. Scr. 99 (2024) 025214.
[30] T. L. Wang, L. Tian, Z. M. Ma, Z. D. Yang, H. W. Han, Bifurcation soliton solutions, M-lump, breather waves, and interaction solutions for (3+1)-dimensional P-type equation, Chaos Soliton Fract. 192 (2025) 115932.
[31] B. Q. Li, Y. L. Ma, Optical soliton resonances and soliton molecules for the Lakshmanan-Porsezian-Daniel system in nonlinear optics, Nonlinear Dynam. 111 (2023) 6689-6699.
[32] K. M. Elhadj, A. Boudjemaa, Equilibrium and scattering properties of a nonlocal three-soliton molecule in Bose-Einstein condensates with competing nonlinearities, Phys. Scr. 96 (2021) 025212.
[33] X. Wang, J. Wei, Antidark solitons and soliton molecules in a (3+1)-dimensional nonlinear evolution equation, Nonlinear Dynam. 102 (2020) 363-377.
[34] S. Y. Lou, Soliton molecules and asymmetric solitons in three fifth order systems via velocity resonance, J. Phys. Commun. 4 (2020) 041002.
[35] Z. W. Yan, S. Y. Lou, Soliton molecules in Sharma-Tasso-Olver-Burgers equation, Appl. Math. Lett. 104 (2020) 106271.
[36] X. Y. Yang, R. Fan, B. Li, Soliton molecules and some novel interaction solutions to the (2+1)-dimensional B-type Kadomtsev-Petviashvili equation, Phys. Scr. 95 (2020) 045213.
[37] J. J. Dong, B. Li, M. W. Yuen, Soliton molecules and mixed solutions of the (2+1)-dimensional bidirectional Sawada-Kotera equation, Commun. Theor. Phys. 72 (2020) 025002.
[38] D. H. Xu, S. Y. Lou, Dark soliton molecules in nonlinear optics, Acta Physica Sinica 69 (2020) 014208.
[39] X. Wang, J. N. Li, L. Wang, J. f. Kang, Dark-dark solitons, soliton molecules and elastic collisions in the mixed three-level coupled Maxwell-Bloch equations, Phys. Lett. A 432 (2022) 128023.
[40] C. C. Ding, Q. Zhou, H. Triki, Z. H. Hu, Interaction dynamics of optical dark bound solitons for a defocusing Lakshmanan-Porsezian-Daniel equation, Opt. Express 30 (2022) 40712-40727.
[41] S. V. Manakov, V. E. Zakharov, L. A. Bordag, A. R. Its, V. B. Matveev, Two-dimensional solitons of the Kadomtsev-Petviashvili equation and their interaction, Phys. Lett. A 63 (1977) 205-206.
[42] W. X. Ma, Y. Zhou, Lump solutions to nonlinear partial differential equations via Hirota bilinear forms, J. Differ. Equations 264 (2018) 2633-2659.
[43] H. A. Lin, L. M. Ling, Large-time lump patterns of Kadomtsev-Petviashvili I equation in a plasma analyzed via vector one-constraint method, J. Math. Phys. 65 (2024) 043505.
[44] J. C. Chen, Y. Chen, B. F. Feng, K. Maruno, Rational solutions to two- and one-dimensional multicomponent Yajima-Oikawa systems, Phys. Lett. A 379 (2015) 1510-1519.
[45] J. G, Rao, K. Porsezian, J. S. He, T. Kanna, Dynamics of lumps and dark-dark solitons in the multi-component long-wave-short-wave resonance interaction system, Proc. A 474 (2018) 20170627.
[46] C. C. Hu, B. Tian, H. M. Yin, C. R. Zhang, Z. Zhang, Dark breather waves, dark lump waves and lump wave-soliton interactions for a (3+1)-dimensional generalized Kadomtsev-Petviashvili equation in a fluid, Comput. Math. Appl. 78 (2019) 166-177.
[47] A. M. Wazwaz, L. Kaur, New integrable Boussinesq equations of distinct dimensions with diverse variety of soliton solutions, Nonlinear Dyn. 97 (2019) 83-94.
[48] N. H. M. Shahen, M. Al Amin, M. M. Uddin, M. M. Rahman, Wave modelling of (3+1)-dimensional Wazwaz Kaur Boussinesq equation with the bilinear neural network method, Sci. Rep. 15 (2025) 33528.
[49] M. Nadeem, A. Islam, M. Senol, Y. Alsayaad, The dynamical perspective of soliton solutions, bifurcation, chaotic and sensitivity analysis to the (3+1)-dimensional Boussinesq model, Sci. Rep. 14 (2024) 9173.
[50] K. S. Nisar, R. Silambarasan, Jacobi elliptic solutions, bright, compound bright-complex singular solitons of (3+1)-dimensional Wazwaz Kaur Boussinesq equation, Opt. Quant. Electron. 56 (2024) 1301.
[51] H. F. Ismael, The (3+1)-dimensional Boussinesq equation: Novel multi-wave solutions, Results Phys. 53 (2023) 106965.
[52] Y. J. Niu, Q. L. Yuan, B. Ghanbari, Z. Zhang, Y. L. Cao, Collision dynamics of high-order localized waves in a novel (3+1)-dimensional integrable Boussinesq model, Results Phys. 56 (2024) 107223.
[53] T. Xu, Y. N. Shan, Wronskian solutions for the (3+1)-dimensional Wazwaz-Kaur-Boussinesq equation, Appl. Math. Lett. 173 (2026) 109769.
[54] M. Senol, B. Ghanbari, Exploration of novel traveling wave solitons to the conformable (3+1)-dimensional Wazwaz-Kaur-Boussinesq equation, Int. J Theor. Phys. 64 (2025) 151.
[55] R. Hirota, The direct method in soliton theory, Cambridge University Press, 2004.
[56] J. W. Miles, Obliquely interacting solitary waves, J. Fluid Mech. 79 (1977) 157.
[57] K. Sakkaravarthi, T. Kanna, Multicomponent long-wave-short-wave resonance interaction system: Bright solitons, energy-sharing collisions, and resonant solitons, Phys. Rev. E 90 (2014) 052912.